5-2014

Thermal Response Characterization and Low Fluid Velocity Measurements Using Specialized In-Situ Thermocouples Via The Loop Current Step Response Method

Alexander Hashem Hashemian
University of Tennessee - Knoxville, ahashemi@utk.edu

To the Graduate Council:

I am submitting herewith a thesis written by Alexander Hashem Hashemian entitled "Thermal Response Characterization and Low Fluid Velocity Measurements Using Specialized In-Situ Thermocouples Via The Loop Current Step Response Method." I have examined the final electronic copy of this thesis for form and content and recommend that it be accepted in partial fulfillment of the requirements for the degree of Master of Science, with a major in Mechanical Engineering.

Majid Keyhani, Major Professor

We have read this thesis and recommend its acceptance:

Jay I. Frankel, Zhili Zhang

Accepted for the Council:
Carolyn R. Hodges

Vice Provost and Dean of the Graduate School

(Original signatures are on file with official student records.)

Thermal Response Characterization and Low Fluid Velocity Measurements Using Specialized In-Situ Thermocouples Via The Loop Current Step Response Method

A Thesis Presented for the
Master of Science
Degree
The University of Tennessee, Knoxville

Alexander Hashem Hashemian

May 2014

DEDICATION

This work is dedicated to my parents, Nazzy and Hashem, who have supported me throughout my academic career and given me wonderful opportunities in life. Their unwavering love has given me strength and inspiration to succeed in my endeavors. I am fortunate to have both of them in my life.

This is also dedicated to my little sister, Nikki, who has gone above and beyond as a sibling and whom I owe much gratitude. She has been a tremendous source of encouragement and support. I hope that I can repay her for all the times she has been there for me.

ACKNOWLEDGMENTS

First and foremost, I would like to thank my academic mentor, Dr. Majid Keyhani, for his time and consideration. In the three years I spent as his student, he taught me heat transfer, how to be a careful experimentalist, and how to look at problems in life from multiple perspectives. He spent countless hours helping me learn the fundamentals and teaching me how to interrogate nuances of the problem at hand by carefully and completely understanding the physics of the system. His unique methodology has given me insight into a more complete approach to science and has made me a better engineering student. I thank Dr. Keyhani for giving me the opportunity to work for him and learn from him. I enjoyed our time in the laboratory discussing heat transfer and brainstorming ideas for experiments. I would also like to thank Dr. Jay Frankel for all the support he has given me. His enthusiasm and interest to help me understand numerical methods and how to properly analyze data made learning such subjects less daunting. He was always available for an impromptu lesson and eager to pass along his wealth of knowledge.

Thank you to my committee member, Dr. Zhili Zhang, for his consideration and assistance. Thank you to NASA (Contract Number: NNX10AN35A) for financially supporting my research work. I thank my father, Dr. H.M. Hashemian, for his time and resources related to this field of study. I thank Dennis Higdon and Daniel Graham, for helping me with the construction of my setup. I thank Bryan Elkins and Andrew Stubblefield for passing along their knowledge. I thank my fellow graduate students Dominik Bottlaender, Yinyan Chen, Hongchu Chen, and Abhay Pande for all the help they have given me. I thank Kelsey Winstead Turley for her patience while sharing a laboratory space with me and for her steadfast companionship. She is an incredibly diligent worker, a thorough and careful student, and an excellent study partner. I am happy to have had the opportunity to work and learn alongside her. Lastly, a special thanks to Jake Plewa for teaching me how to write code, how to configure data acquisition boards, how to make thermocouples, and how to perform innumerable other tasks in the laboratory. He was an excellent teacher, and I cannot emphasize enough how much I learned from him. I am truly grateful for the skills I have adopted from Jake. I thank him for all the time he spent explaining his work to me and helping me with my own. Mostly importantly, I thank him for his friendship.

ABSTRACT

In this study, a specialized balanced-leads thermocouple was developed to perform in-situ thermal response characterization via the LCSR test method. Thermal response characterization of installed thermocouples is essential in order to obtain accurate positional temperature data in rapid transient applications. An analytical model is presented that fully describes the thermocouple system based on a first-principles approach to the heat transfer physics of the sensor. In conjunction with the LCSR test, the full model presented yields quantifiable characterization parameters useful for determining accurate positional temperature data. It is necessary to employ a balanced-leads thermocouple for this experimental procedure in order to ensure that the thermocouple bead and its leads are at the same initial temperature, when performing the LCSR test. If the installed thermocouple is in a fluid domain, it has been demonstrated that the LCSR test data may be calibrated against the fluid velocity. This finding was verified by comparison of the present experimental data with forced convection correlations obtained by previous researchers. The next task to improve the work of this study is to construct a balanced-leads thermocouple with a lead temperature ratio of unity. This new balanced-leads thermocouple will more closely satisfy the assumptions made for applying the full model to the thermocouple system. For this study, the data obtained was compared with previous researchers' convection correlations to demonstrate a proof of concept. Lastly, the thermocouple sensor should be calibrated carefully over a wider velocity range before it can be implemented in an industrial application. This calibration procedure must be repeated for each individual thermocouple sensor to be installed. If these additional tasks are performed, a balanced-leads thermocouple characterized via the LCSR test method could become a valuable and versatile temperature-velocity probe for industrial processes.

TABLE OF CONTENTS

LIST OF TABLES

LIST OF FIGURES

NOMENCLATURE

a = LCSR data analysis parameter, $\frac{\tau_0}{2\lambda^2}$, (-)

$A_{c,lead,i}$ = Cross-Sectional Area of Thermocouple Lead Wire i (i = 1, 2), (m^2)

A_s = Surface Area of Thermocouple Bead, (m^2)

b = LCSR data analysis parameter, $\frac{2\lambda}{\tau_0}$, ($s^{-1/2}$)

B_n = Coefficients for Response Equation (Carroll and Shepard), (K)

C_{lead} = Specific Heat Capacity of the Lead Wire, ($kJkg^{-1}K^{-1}$)

C_{TC} = Specific Heat Capacity of Thermocouple Bead, ($kJkg^{-1}K^{-1}$)

D = Thermocouple Bead Diameter, (m)

d = Diameter of Thermocouple Lead Wire i (i = 1, 2), (m)

$\dot{E}$ = Rate of Energy Transfer, (W)

Gr_D = Grashoff Number of Thermocouple Bead, $\frac{g\beta D^3 \Delta T_{TC}}{\nu^2}$, (-)

g = Acceleration of Gravity, (ms^{-2})

h = Effective Heat Transfer Coefficient, ($Wm^{-2}K^{-1}$)

i = Electrical Current, (A)

k = Thermal Conductivity, ($Wm^{-1}K^{-1}$)

k_{lead} = Thermal Conductivity of the Lead Wire, ($Wm^{-1}K^{-1}$)

L = Length of the Lead Wire, (m)

LCSR = Loop Current Step Response

m = Mass, (kg)

m_{lead} = Mass of the Lead Wire, (kg)

M_a = Mean of the *a* Array, $a = \frac{\tau_0}{2\lambda^2}$, (-)

Nu_D = Nusselt Number of Thermocouple Bead, $\frac{hD}{k}$, (-)

P(t) = Response of a Thermocouple (Carroll and Shepard), (K)

Pr = Prandtl Number, $\frac{\nu}{\alpha}$, (-)

$q_{lead,i}$ = Conduction Heat Loss/Gain per Unit Cross-Sectional Area of Lead Wire i (i = 1, 2), (Wm^{-2})

R = Electrical Resistance, (Ω)

$\Re$ = Residual between LCSR Data and Full Model, (-)

$\Re_f$ = Residual between LCSR Data and First-Order Model, (-)

$\overline{\Re}$ = Mean of Residual, (-)

Ra_D = Rayleigh Number of Thermocouple Bead, Gr_DPr, (-)

Re_D = Reynolds Number of Thermocouple Bead, $\frac{v_{air}D}{\nu}$, (-)

r = Electrical Resistivity, (Ωm)

t = Time, (s)

t_{cr} = Critical Time, (s)

Δt = LCSR Heating Duration, (s)

T = Temperature, (°C)

T_∞ = Ambient Temperature, (°C)

TC = Thermocouple

T_{TC} = Thermocouple Temperature, (°C)

$\dot{T}_{TC}$ = Time Rate of Change of Thermocouple Temperature, ($°Cs^{-1}$)

ΔT_{TC} = Change in Thermocouple Temperature, (°C)

ΔT_{lead} = Change in Thermocouple Lead Wire Temperature, (°C)

V_{TC} = Volume of Thermocouple Bead, (m^3)

v_{air} = Air Velocity, (ms^{-1})

Greek

α = Thermal Diffusivity, (m^2s^{-1})

β = Isobaric Coefficient of Thermal Expansion, (K^{-1})

θ(t) = Normalized Temperature, (-)

θ_{TC} = Dimensionless Thermocouple Temperature, $\theta_{TC}(t) = \frac{T_{TC}(t) - T_\infty}{T_{TC}(0) - T_\infty}$, (-)

λ = Thermocouple Leads Axial Conduction Heat Loss/Gain Parameter, ($s^{1/2}$)

μ = Dynamic Viscosity, ($kgs^{-1}m^{-1}$)

ν = Kinematic Viscosity, (m^2s^{-1})

ρ_{lead} = Density of the Lead Wire, (kgm^{-3})

ρ_{TC} = Density of Thermocouple Bead, (kgm^{-3})

σ = Standard Deviation, (-)

σ_a = Standard Deviation of the *a* Array, $a = \frac{\tau_0}{2\lambda^2}$, (-)

τ_{TC} = Thermocouple Decay Response Characteristic Function as Defined by Eq. (2.1.15), (s)

τ = Time Constant Without Axial Conduction, (s)

τ_0 = Time Constant With Axial Conduction, (s)

τ_{max} = Maximum Time Constant, (s)

CHAPTER 1: INTRODUCTION

1.1 Background

A thermocouple (TC) can be used to provide temperature data in various mediums. TCs are widely used in various industrial applications. However, unless the process is steady state and the leads of the TC are along the isotherm, the measured temperature of the TC is different from the temperature of the target host. In order to correct for this discrepancy, the thermocouple must be characterized. For steady state conditions in which the lead wires are not parallel to the isotherm, the difference between the target temperature and the TC temperature is due to axial conduction along the lead wires. For transient measurements, the problem is worsened by the response time of the thermocouple. The orientation of the TC leads with respect to the isotherm is important and must be considered when pursuing a response characterization technique.

Consider the installed thermocouple orientations shown in Figure 1.1.1, which displays one TC installed with its leads normal to the isotherm and another TC installed with its leads parallel to the isotherm. If the surface heat flux is uniform, the TC situated normal to the isotherm will experience conductive lead loss effects. Therefore, the characterization technique must account for the response time of the TC bead as well as these lead losses. However, the TC oriented parallel to the isotherm will not experience any conductive lead loss effects. This is an idealization based on the assumption of negligible temperature difference between the TC bead and its lead wires. Thus, the characterization technique for a TC whose leads are parallel to the isotherm would only need to account for the response time of the thermocouple bead.

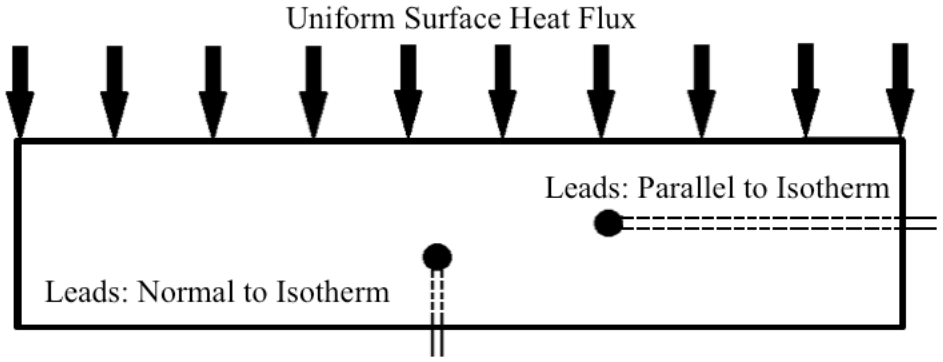

Figure 1.1.1 Diagram demonstrating thermocouple lead wire orientations.

Thermal protection systems (TPS) of hypersonic flight vehicles, engine combustion, and fire research applications utilize TCs installed in a solid material. The pertinent inverse heat conduction analysis requires accurate in-depth positional temperature data in order to predict thermal conditions at boundaries of interest, such as surface heat flux and surface temperature. Therefore, characterization of an installed TC is vital to solving inverse heat conduction problems. Thermocouple manufacturers often report measured response time for the probes when the probe is subjected to a step change in water or air flowing at some velocity. This response information is only valid when the end user subjects the TC probes to the exact test conditions performed by the manufacturer. Therefore, the characteristics of the TC probes must be determined after the user installs them. The Loop Current Step Response (LCSR) test method has been used for years in the nuclear energy industry to characterize the response of installed resistance temperature detectors (RTDs). It will be shown that the method is capable of determining accurate response data from in-situ TCs. Additionally, if the TC is installed in a fluid domain, its response data obtained from LCSR can be correlated to determine low flow velocity measurements.

1.2 Literature Review

As mentioned in the previous section, LCSR was developed to measure the in-situ transient response of temperature sensors such as thermocouples. The LCSR method outlined by Carroll and Shepard [1] specifies that an electric current is passed through the sensor circuit until the sensor attains a steady state temperature, then the current is turned off, and finally the time dependence of the cooling is analyzed to predict the transient response. The decay response data collected from LCSR was compared to that of plunge tests on the same TC. The TC decay data was analyzed using a response model of the form:

$$P(t) = B_0 + B_1 e^{-t/\tau_1} + B_2 e^{-t/\tau_2} + \ldots \tag{1.2.1}$$

Carroll and Shepard found that only the first two or three terms of Eq. (1.2.1) have practical significance because experimental data contains noise and their computer-fitting program could not resolve the very small influence of the higher terms.

A TC is comprised of two dissimilar metal wires, which are welded together to form the measuring junction or bead. The dissimilar metals have different electrical resistances and thermal capacitances. The lead wires are connected in series and therefore will share the same current. Resistive joule heating is a function of both electrical current and resistance. Passing current through the thermocouple will result in one lead wire at a higher temperature than the other. However, in an actual application, the TC leads are at the same temperature. Therefore, the uneven lead temperatures that results from an LCSR test is an artifact that must be overcome. Therefore, a TC must be modified in order for the sensor to be conducive to LCSR response characterization. By adjusting the TC lead wire diameters to account for their uneven electrical resistances and thermal capacitances, a "balanced TC" may be constructed that is amenable to the LCSR method and yields valuable response information. This subject along with the specific obstacles involved with performing LCSR on a TC is discussed further in Section 2.2.

Measuring low fluid velocities (<100 cm/s) is difficult and existing methods are prone to complications that compromise accuracy. Hot-wire anemometers are commercially available probes that measure fluid flow velocity. The probe is typically small and therefore yields negligible disturbance to flow field and allows for a quick response. In a hot-wire anemometer, the electrically heated sensor is exposed to fluid flow. The current required to maintain a constant temperature difference between the sensor and the fluid is measured. The amount of current provided to the sensor may be calibrated to provide a direct measure of the fluid velocity. It must be noted that the fundamental concept utilized in a hot-wire anemometer is the fact that the convection heat transfer coefficient across the sensor element is a function of fluid velocity. Application of hot-wire anemometry in low fluid velocity domains requires special calibration techniques and considerations due to the challenge of maintaining a uniform velocity profile [2]. Further complications arise when considering the orientation of the probe with respect to flow. For example, a typical handheld hot-wire anemometer that is installed in a horizontal duct measuring low velocity cross flow is subject to local natural convection flow that may alter the desired horizontal cross flow measurements due to forced convection. Some hot-wire anemometers suffer from aging effects and their calibration characteristics can change over time until failure. In order to ensure accurate measurements, the probes should be periodically

checked [3]. However, it may not be possible or convenient to remove the probe from its installation for re-calibration. The complications related to hot-wire anemometry for low flow velocity applications make the prospect of another means quite attractive.

For velocity measurements, a thermocouple bead can be approximated as an isothermal sphere immersed in a fluid. Extensive research has been conducted to obtain heat transfer correlations over a sphere subjected to forced convection. A commonly used correlation for forced convection over an isothermal sphere is proposed by Whitaker [4] of the form

$$\overline{Nu}_D = 2 + (0.4\,\mathrm{Re}_D^{1/2} + 0.06\,\mathrm{Re}_D^{2/3})\,\mathrm{Pr}^{0.4}\left(\frac{\mu}{\mu_s}\right)^{1/4} \tag{1.2.2}$$

$$\begin{bmatrix} 0.71 \le \mathrm{Pr} \le 380 \\ 3.5 \le \mathrm{Re}_D \le 7.6\times10^4 \\ 1.0 \le \left(\frac{\mu}{\mu_s}\right) \le 3.2 \end{bmatrix}$$

where all properties are evaluated at T_∞ (except for μ_s which is evaluated at the surface temperature of the sphere). For this study, the quantity (μ/μ_s) is taken to be equal to one. Ranz and Marshall [5] obtained another correlation that relates to the transport of free falling liquid droplets for $0 < \mathrm{Re}_D < 200$ and $\mathrm{Pr} = 0.71$. Their correlation also be applied to spheres subjected to forced convection and is expressed as

$$\overline{Nu}_D = 2 + 0.6\,\mathrm{Re}_D^{1/2}\,\mathrm{Pr}^{1/3} \tag{1.2.3}$$

Woo [6] conducted a numerical investigation of convection heat transfer for a single sphere in an unbounded fluid domain. His discrete results for forced convection heat transfer from a sphere for $0.05 < \mathrm{Re}_D < 100$ and $\mathrm{Pr} = 0.71$ are tabulated in Table 1.2.1.

Table 1.2.1 Discrete values for Nu_D obtained by the numerical investigation of Woo for various values of Re_D ranging from 0.05-100.

Re_D	0.05	0.1	0.2	0.5	0.75	1.0	2.0	3.0	5.0	10	30	57	100
Nu_D	2.016	2.028	2.058	2.136	2.194	2.246	2.43	2.588	2.844	3.34	4.61	5.75	6.98

Several correlations for natural convection heat transfer from an isothermal sphere have been reported in the literature. The most commonly used correlation for natural convection from an isothermal sphere (for $Ra_D < 10^{11}$ and $Pr \geq 0.7$) comes from Churchill [7] and is of the form

$$\overline{Nu}_D = \frac{0.589 Ra^{1/4}}{\left(1 + (0.469/\mathrm{Pr})^{9/16}\right)^{4/9}} \tag{1.2.4}$$

There are very few explicit correlations reported for mixed convection heat transfer. A common expression used for estimating aiding mixed convection Nusselt number (Nu_M) is given by

$$Nu_M^n = Nu_F^n + Nu_N^n \tag{1.2.5}$$

where Nu_F is the Nusselt number for forced convection and Nu_N is the Nusselt number for natural convection. Some researchers have chosen n = 2 and others have chosen n = 4. Churchill and Ozoe [8] developed correlating equations for natural and forced convection that utilize n = 3. Churchill argues that prior researchers' choice of n = 2 or 4 was based on loose rationalization and was not tested critically. Substituting Eq. (1.2.2) and Eq. (1.2.4) into Eq. (1.2.5) yields a suitable correlation for mixed convection heat transfer from an isothermal sphere to a slow moving fluid.

The correlations for forced convection and the numerical results of Woo are plotted in Figure 1.2.1, along with the mixed convection estimation expression for n = 3, Pr = 0.71, Ra_D = 2.5. Between the forced convection correlations, there is a large relative discrepancy, particularly at low Reynolds numbers. It must be noted that all correlations, obtained from experimental data or numerical investigations, are subject to some level of uncertainty. Nevertheless, Figure 1.2.1 gives insight into the dependence of the heat transfer coefficient (Nu_D) on fluid flow velocity (Re_D).

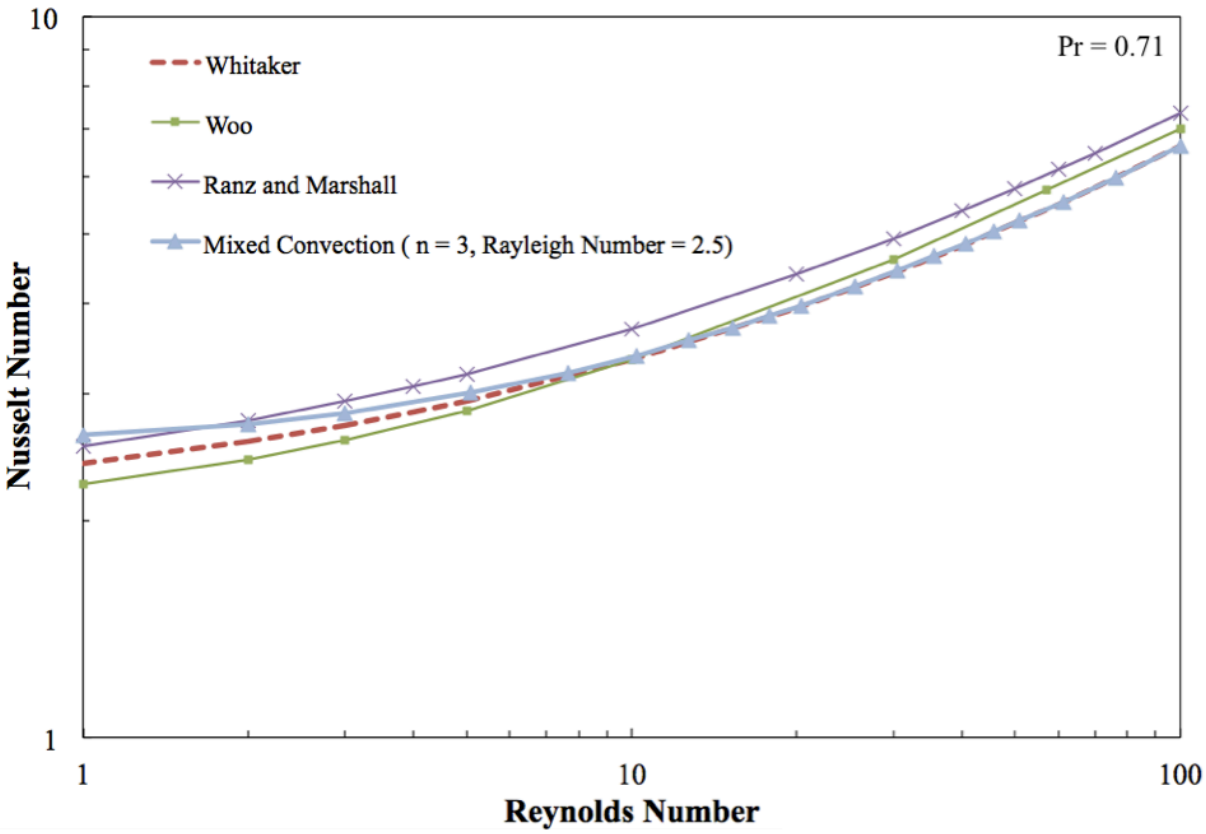

Figure 1.2.1 Comparison of forced convection correlations for Pr = 0.71 along with mixed convection estimation for n = 3, Ra_D = 2.5.

If the LCSR test is performed on a TC subjected to fluid cross flow at some velocity, the thermal response of its decay data can be converted to the Nusselt number of an isothermal sphere immersed in a flowing fluid. By repeating this process at various velocities, a TC may be calibrated to measure fluid flow. Therefore, the utilization of the LCSR method on a balanced thermocouple provides response characterization and velocity measurement simultaneously. The details of LCSR on TCs in a low flow domain will be examined further in Section 4.3.

1.3 Scope

The goal of this research was to provide an experimental and analytical procedure by which a balanced thermocouple's characteristics can be quantified in order to obtain accurate positional temperature data as well as low velocity fluid flow measurements. First, the LCSR method, similar procedures of producing sensor temperature step changes, and the limitations of these methods are studied. Second, a specialized thermocouple is presented that is used to generate response data via LCSR. Next, a new method is presented which accounts for the thermal response of the thermocouple bead as well as the axial conduction effect of the leads. Finally, the response time data obtained from the LCSR test data is correlated with low velocity fluid flow to yield a specialized thermocouple sensor capable of producing more accurate positional temperature data and fluid velocity measurements.

CHAPTER 2: THERMOCOUPLE THEORY

2.1 Governing Equation and Derivation of Response Characteristic Parameters

A lumped capacitance model is used to analyze the response characteristics of the TC. The energy balance of the TC bead for zero volumetric rate of heat generation is given as

$$\dot{E}_{stor} = \dot{E}_{in} + \dot{E}_{gen} - \dot{E}_{out} \tag{2.1.1}$$

The surrounding environment is assumed to be hot and therefore heat transfer is incident from the surroundings to the TC bead. It is also assumed that heat is lost from the bead to the leads (as is the case for a TC installed normal to the isotherm, shown in Fig. 1.1.1). The energy balance from Eq. (2.1.1) may be rewritten as

$$\left(\rho CV\right)_{TC}\dot{T}_{TC}(t) = hA_s\left(T_\infty(t) - T_{TC}(t)\right) - A_{c,lead,1}q_{lead,1}(t) - A_{c,lead,2}q_{lead,2}(t) \tag{2.1.2}$$

where T_{TC} is the TC bead temperature, $\dot{T}_{TC}$ is its rate of change, h is the effective heat transfer coefficient (which includes contact resistance between the bead and the host material), A_s is the surface area of the bead in contact with surroundings, T_∞ is the temperature of the surroundings, $A_{c,lead,1}$ and $A_{c,lead,2}$ are the cross-sectional areas of the lead wires in contact with the bead, $q_{lead,1}$ and $q_{lead,2}$ are the heat losses per unit cross-sectional area from the bead to the each lead wire, ρ_{TC} is the density of the bead, C_{TC} is the specific heat capacity of the bead, and V_{TC} is the volume of the bead.

After rearranging, Eq. (2.1.2) becomes

$$\frac{\left(\rho CV\right)_{TC}}{hA_s}\dot{T}_{TC}(t) + T_{TC}(t) = T_\infty(t) - \frac{A_{c,lead,1}}{hA_{TC}}q_{lead,1}(t) - \frac{A_{c,lead,2}}{hA_{TC}}q_{lead,2}(t) \tag{2.1.3}$$

The constant τ_0 is defined as

$$\tau_0 = \frac{\left(\rho CV\right)_{TC}}{hA_s} \tag{2.1.4}$$

Substituting Eq. (2.1.4) into Eq. (2.1.3) yields

$$\tau_0 \dot{T}_{TC}(t) + T_{TC}(t) = T_\infty(t) - \frac{A_{c,lead,1}}{hA_s} q_{lead,1}(t) - \frac{A_{c,lead,2}}{hA_s} q_{lead,2}(t) \tag{2.1.5}$$

For small time, the lead heat loss from each lead can be described using the half-space integral relationship given by [9]

$$q_{lead,i}(t) = \sqrt{\frac{(\rho C k)_{lead,i}}{\pi}} \int_{u=0}^{t} \dot{T}_{TC}(u) \frac{du}{\sqrt{t-u}}, \qquad i = 1,2 \tag{2.1.6}$$

where subscript *i* refers to lead wires one and two.

The constant λ is defined as

$$\lambda = \frac{1}{hA_s} \left[A_{lead,1} \sqrt{\frac{(\rho C k)_{lead,1}}{\pi}} + A_{lead,2} \sqrt{\frac{(\rho C k)_{lead,2}}{\pi}} \right] \tag{2.1.7}$$

Eq. (2.1.7) clearly shows that λ must be positive and indeed is an intrinsic property of the installed TC. Substituting Eqs. (2.1.6 and 2.1.7) into Eq. (2.1.5) yields

$$\tau_0 \dot{T}_{TC}(t) + T_{TC}(t) = T_\infty(t) - \lambda \int_{u=0}^{t} \dot{T}_{TC}(u) \frac{du}{\sqrt{t-u}} \tag{2.1.8}$$

The directionality of heat transfer between the TC bead and its leads is determined by the sign of $\dot{T}_{TC}$. Further insight regarding the behavior of the lead loss/gain term can be gained by expanding $\dot{T}_{TC}(u)$ about *t* in Eq. (2.1.6), which results in

$$\int_{u=0}^{t} \dot{T}_{TC}(u) \frac{du}{\sqrt{t-u}} = 2t^{1/2} \dot{T}_{TC}(t) + \frac{4}{3} t^{3/2} \ddot{T}_{TC}(t) + O(t^{5/2}) \tag{2.1.9}$$

Substituting only the first-order term from Eq. (2.1.9) into Eq. (2.1.8) yields

$$\left(\tau_0 + 2\lambda\sqrt{t}\right) \dot{T}_{TC}(t) + T_{TC}(t) \approx T_\infty(t) \tag{2.1.10}$$

Therefore, including the lead loss/gain term in Eq. (2.1.8) yields the TC decay response characteristic function given by

$$\tau_{TC}(t) = \tau_0 + 2\lambda\sqrt{t} \tag{2.1.11}$$

Assuming T_∞ is constant, Eq. (2.1.10) has an exact solution via Laplace Transform (derivation found in Appendix A.1) of the form

$$\theta_{TC}(t) \approx \exp\left\{\frac{1}{2\lambda^2}\left[\tau_0 \ln\left(\tau_0 + 2\lambda\sqrt{t}\right) - \tau_0 \ln\left(\tau_0\right) - 2\lambda\sqrt{t}\right]\right\}, \quad t \geq 0, \tag{2.1.12}$$

Where $\theta_{TC}(t)$ is dimensionless temperature

$$\theta_{TC}(t) = \frac{T_{TC}(t) - T_\infty}{T_{TC}(0) - T_\infty} \tag{2.1.13}$$

It is clear that Eq. (2.1.10) reduces to a first-order system if lead losses are negligible ($\lambda \approx 0$). This is an ideal case for a thermocouple whose leads are parallel to the isotherm. The exact solution to a first-order system is given by

$$\theta_{TC}(t) = \exp\left(-\frac{t}{\tau_0}\right), \quad t \geq 0. \tag{2.1.14}$$

In most practical in-situ applications, λ is greater than zero. Therefore, the thermocouple decay response characteristic function may be approximated as a piecewise function that increases from τ_0 to some $\tau_{\max}$ value at $t = t_{cr}$:

$$\tau_{TC}(t) = \begin{cases} \tau_0 + 2\lambda\sqrt{t} & t \leq t_{cr} \quad \text{(2.1.15 a)} \\ \tau_{\max} = \tau_0 + 2\lambda\sqrt{t_{cr}} & t > t_{cr} \quad \text{(2.1.15 b)} \end{cases}$$

where t_{cr} is given by

$$t_{cr} = \left(\frac{\tau_{\max} - \tau_0}{2\lambda} \right)^2 \tag{2.1.16}$$

It has been demonstrated by Elkins [10] that Eq. (2.1.15) can be utilized to provide a full model for a thermocouple response. By incorporating Eq. (2.1.12) as a good decay model for $t < t_{cr}$ with Eq. (2.1.14) as a good decay model for $t > t_{cr}$, the full model for a thermocouple response may be obtained:

$$\theta_{TC}(t) = \begin{cases} \exp\left\{ \frac{1}{2\lambda^2} \left[\tau_0 \ln\left(\tau_0 + 2\lambda\sqrt{t} \right) - \tau_0 \ln(\tau_0) - 2\lambda\sqrt{t} \right] \right\}, & t \le t_{cr} \\ \exp\left\{ \frac{1}{2\lambda^2} \left[\tau_0 \ln\left(\tau_0 + 2\lambda\sqrt{t_{cr}} \right) - \tau_0 \ln(\tau_0) - 2\lambda\sqrt{t_{cr}} - 2\lambda^2 \frac{t - t_{cr}}{\tau_{\max}} \right] \right\}, & t > t_{cr} \end{cases} \tag{2.1.17}$$

The thermocouple decay response characteristic function of an in-situ thermocouple is a function of the sensor's thermophysical properties, its geometry, the contact resistance between the sensor and the host material, and conductive lead losses. In summary, it is clear that in order to characterize an in-situ TC, values for τ_0, λ, and t_{cr} (or τ_{max}) must be obtained from LCSR test decay data.

2.2 Challenges of Applying LCSR to Thermocouples

LCSR requires the passing of an electric current through a sensor's circuit for some time with the intention of raising the temperature of the sensor above the ambient environment. After the current is turned off, the sensor is allowed to decay back to its initial condition. This decay transient can be analyzed to determine the dynamic response of the sensor. Previous researchers understood the challenges that came with applying the LCSR method to TCs. LCSR's success in the nuclear energy industry is mainly due to its ease of utilization on resistance temperature detectors (RTDs). The sensing element of an RTD is a platinum coil of large electrical resistance

relative to the sensor's lead wires, which are of identical low resistance material. Therefore, passing an electric current through the RTD results in a large temperature rise in the sensing element only. The result of this phenomenon is a relatively accurate representation of the thermal response of the RTD. For a TC, the sensing element is the welded junction of two dissimilar metal wires with dissimilar electrical resistances and thermal capacitances. The junction or bead of the TC itself has a small electrical resistance relative to its leads. Hence, as a result of performing LCSR on a TC, one lead wire will be at a higher temperature than the other lead wire and the TC bead will be at some intermediate temperature. When the current is removed from the sensor's circuit, the sensor will yield a transient decay back to its initial conditions. However, this decay is not representative of the actual physics that an installed sensor experiences. Therefore, the response parameters obtained from analyzing this decay data are corrupted by the artifact of the LCSR test.

CHAPTER 3: EXPERIMENTAL SETUP AND PROCEDURE

3.1 Setup and Procedure Design

LCSR Test Apparatus. Figure 3.1.1 shows a diagram of the electrical circuit used to perform the LCSR test on thermocouples. Initially, TC data is collected at ambient temperature by the data acquisition system (Data Translation Model: 9824). After some time, the solid-state relay of the DT9824 activates the positive leg of the power supply connected to the mechanical relay coil. The coil then energizes to engage two switches simultaneously to initiate current flow to the TC. The current supplied by the power supply may be limited to an amount specified by the operator that is suitable for the wire gauge of the circuitry. As the current flows through the thermocouple leads and bead, the sensor's temperature rises. After a short period of time, the solid-state relay is deactivated, which in turn, de-energizes the mechanical relay coil to halt the current flow through the thermocouple circuit. As a result of this procedure, the thermocouple is now at an elevated temperature relative to its ambient. At this time, the thermocouple begins to decay back to its initial temperature. During the entirety of this process, the electromotive force (emf) signal of the thermocouple is recorded at a sampling rate of 200 Hz and a gain of 32 and stored by the data acquisition system for analysis. Photos of the experimental setup are included in Appendix A.2.

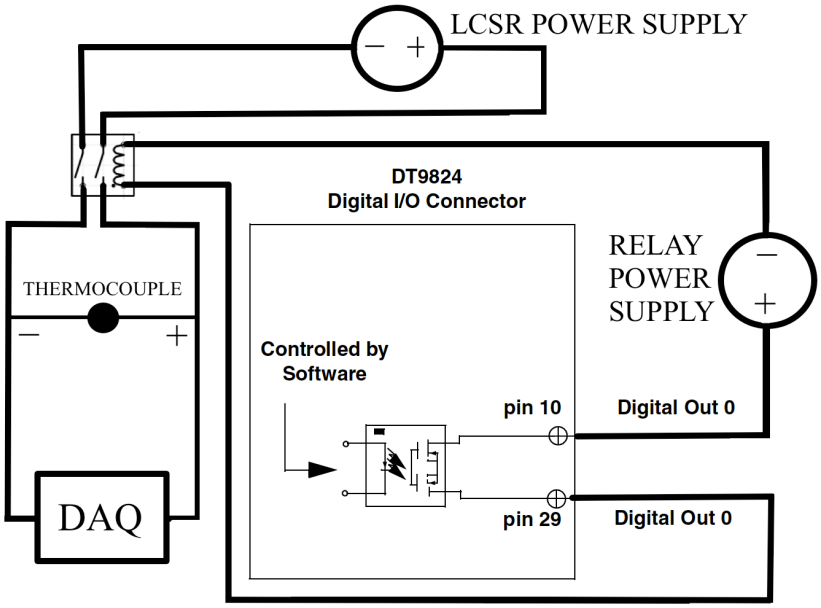

Figure 3.1.1 Schematic of LCSR circuit used in experimentation.

Velocity Calibration Test Apparatus. In order to collect decay data for thermocouples in cross flow, a flow channel was constructed using an acrylic circular tube (length = 24 ¼ inches, inside diameter = 2 ⅝ inches) and a small electrically powered fan (Delta Electronics, Inc. Model: AFB0812VHB). The fan draws in air through the tunnel so that at the entrance of the flow channel, the air velocity profile is uniform as shown in Figure 3.1.2a. The thermocouple is positioned at the entrance of the flow channel along with a hot-wire anemometer (TSI VelociCalc 8345), which is used to measure the air velocity at the entrance, as seen in Figure 3.1.2b. The aforementioned LCSR test procedure was conducted and repeated for various air velocities. After each set of LCSR decay data was analyzed, a correlation between the thermocouple response and the air velocity was obtained. These results will be presented and discussed further in Chapter 4. A photograph of the flow channel is included in Appendix A.2.

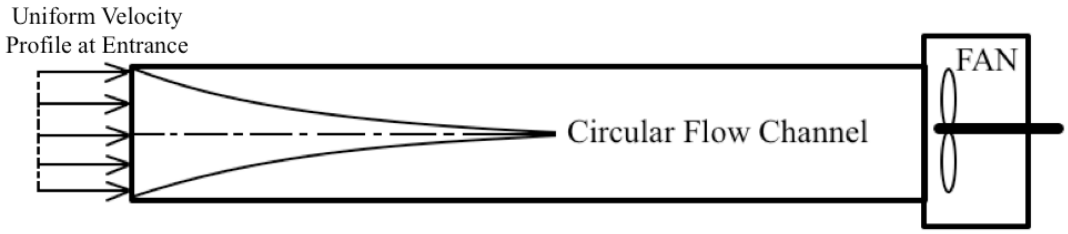

Figure 3.1.2a Side view of the flow channel used to calibrate TC response data to air velocity.

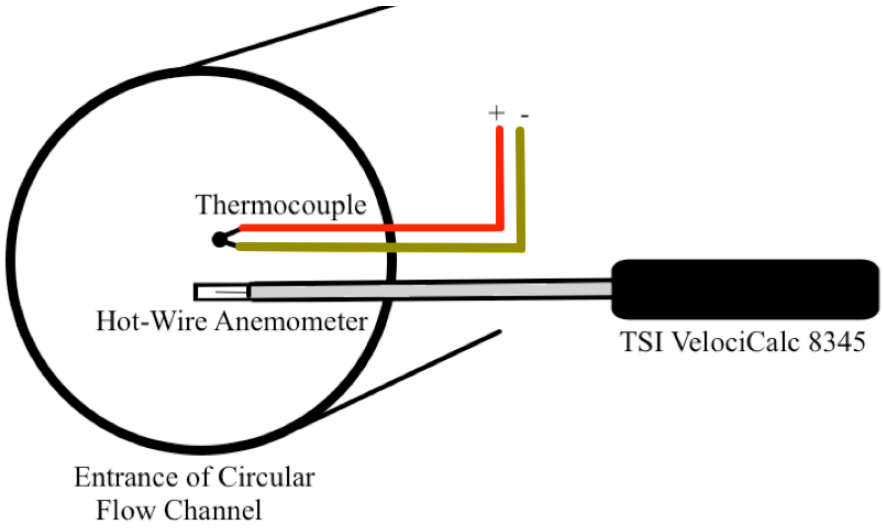

Figure 3.1.2b Diagram of the flow channel entrance.

Figure 3.1.3 demonstrates a typical plot of the data collected from conducting LCSR on a balanced-leads thermocouple (K2) that is immersed in slow-moving room temperature air with its lead wires covered with insulation. In this specific LCSR test run, there are five seconds of initial temperature data. After five seconds, the relays have been triggered to allow for heating to take place at a current of 2.0 A. The duration of the LCSR heating was selected to be five seconds. Although this duration is somewhat arbitrary, it should be noted that a short heating period is desirable, because it ensures that the ambient temperature is not disturbed. In this example, the air is continuously moving across the thermocouple and therefore the temperature of the ambient may be assumed to be constant. If the air was stagnant, a shorter heating period should have been specified. Basic knowledge of the heat transfer coefficient for a given situation gives insight to the operator when choosing the heating duration. After the heating period, the thermocouple decays back to its initial condition.

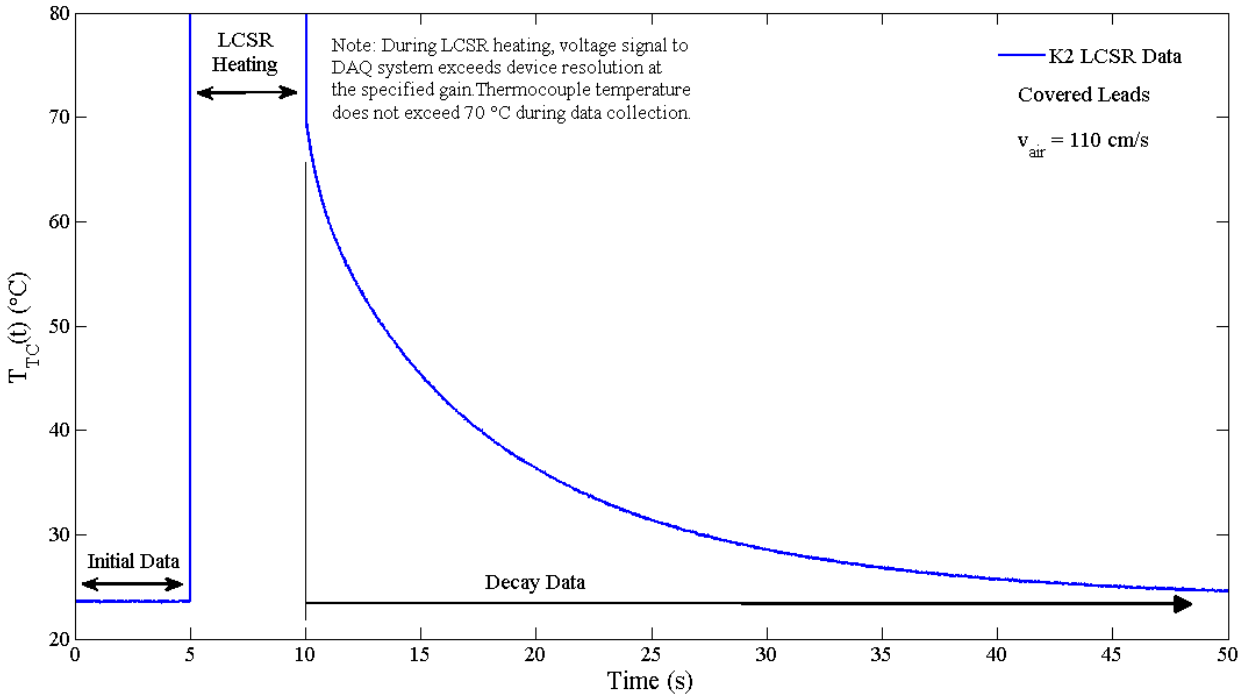

Figure 3.1.3 Example plot of LCSR test data.

For response characterization, the decay portion of the data is of particular interest. Once the data is recorded and saved, the initial data and heating period data are removed. Now, only the decay data remains with the peak of the data being the maximum temperature of the sensor. After subtracting the value for the initial temperature from the decay data, the data is now expressed in terms of the change in temperature of the thermocouple. In addition, the time scale is adjusted to remove the initial data and heating periods, as it is shown in Figure 3.1.4. Further, the decay data may be made dimensionless and plotted as a normalized signal ranging from one to zero.

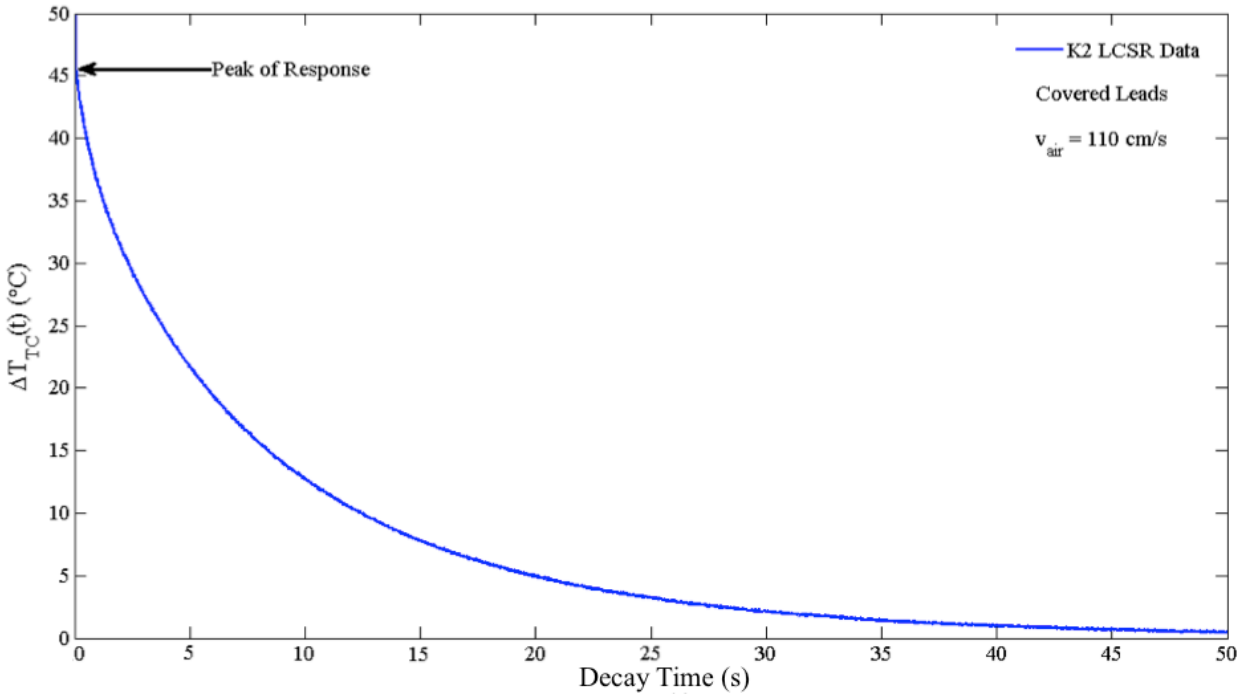

Figure 3.1.4 LCSR decay data expressed as the change in thermocouple temperature over time.

3.2 Design of Balanced-Leads Thermocouple

The primary challenge of performing the LCSR test on a thermocouple is that when the current supplied to the sensor circuit is removed, the leads and the bead are not at the same elevated temperature. More specifically, the lead with the higher electrical resistance will be at some elevated temperature, the lead with the lower electrical resistance will be at a lower elevated temperature, and the bead will be at some intermediate temperature between the two. As the thermocouple is allowed to cool and decay back to its initial condition, some heat transfers from the higher temperature lead across the bead and toward the lead at lower temperature. In contrast, the analysis of the sensor data assumes that the entire thermocouple is at the same elevated temperature before it begins to cool.

Standard commercial thermocouples are composed of two dissimilar metal wires of equal diameter that are welded together to form a bead. There are various types of thermocouples composed of different metal lead wire pairings. Selecting a thermocouple type depends on cost, availability, convenience, temperature range, chemical properties, stability, sensitivity, and output. The most common characteristics of interest when selecting a thermocouple type are temperature range and sensitivity. For the purpose of this study, a Type-K thermocouple was analyzed. Type-K (Chromel-Alumel) thermocouples are the most common general-purpose thermocouple with a wide temperature range and good sensitivity.

In order to overcome the uneven heating that takes place when performing the LCSR test on a thermocouple, it is necessary to construct a modified thermocouple that accounts for this heating discrepancy. The lead temperature differences stem from the dissimilarities in the thermophysical properties of the lead wire metals. However, by adjusting the dimensions of the lead wire diameters, it is possible to balance the lead temperatures so that the entire sensor is at a uniform elevated temperature at the start of its decay response.

The temperature increase of a lead wire due to joule heating may be expressed as

$$\Delta T_{lead} = \frac{i^2 R \Delta t}{(mC)_{lead}} \tag{3.2.1}$$

Where i is the current supplied, R is the electrical resistance of the lead wire metal, Δt is the heating time duration, m_{lead} is the mass of the lead wire, and C_{lead} is the specific heat capacity of the lead wire. In order to balance the temperature increase of the leads, the following equality must be satisfied

$$\Delta T_{lead,1} = \Delta T_{lead,2} \tag{3.2.2}$$

where subscripts 1 and 2 refer to lead wire one and lead wire two, respectively. With minor manipulation ($m = \rho L A_{c,lead}$, $A_{c,lead} = \pi d^2/4$, ρ = density, L = length of the lead wire, d = diameter of the lead wire), Eq. (3.2.2) may be rewritten as

$$\left(\frac{r}{\rho C d^4}\right)_1 = \left(\frac{r}{\rho C d^4}\right)_2 \tag{3.2.3}$$

where $r = RA_c/L$ is the electrical resistivity of the lead wire.

Eq. (3.2.3) can be applied to any thermocouple. By adjusting the diameters, the change in lead temperatures can be made equal. It should be noted that there are limitations to utilizing this equality. Firstly, in order to obtain a perfect balance, exact values for wire diameters must be selected, which may not be available from manufacturers. Therefore, for this study, the closest diameters commercially available were used to balance the lead temperatures. Secondly, although Eq. (3.2.3) may be applied to any thermocouple type, some types may be more suitable than others. For example, in order to balance the lead temperatures of a Type-T thermocouple (Copper-Constantan), the constantan wire would need to be 2.3 times larger than that of the copper wire. This makes welding a bead more difficult and makes the sensor more fragile. Lastly, Eq. (3.2.3) assumes that the lead wire properties are constant and well known. Any discrepancy may lead to an uneven balance.

A Type-K thermocouple (designated as thermocouple K2) was constructed using 24AWG chromel wire and 26AWG alumel wire. Given the availability of these wire diameters and the thermophysical properties of chromel and alumel, a reasonable balance and a suitable ratio of diameters were obtained. Wire properties were obtained from the manufacturer (OMEGA) and are presented in Table 3.2.1.

Table 3.2.1 Thermophysical properties of Type-K Lead Metals

Property	Chromel	Alumel
Electrical Resistivity (Ωm)	7.06E-07	2.94E-07
Density (kg/m^3)	8730	8600
Mass Specific Heat Capacity [kJ/(kgK)]	0.448	0.5233
Thermal Conductivity [W/(mK)]	19.3	29.7

Satisfying Eq. (3.2.3) for a standard Type-K thermocouple yields a poor lead temperature ratio of 0.362. The balanced Type-K thermocouple K2, consisting of a 24AWG chromel wire and 24AWG alumel wire, yields a more favorable temperature ratio of 0.917.

Table 3.2.2 Lead temperature ratios for a standard 24AWG Type-K thermocouple and balanced thermocouple K2 (where subscripts *a* and *c* refer to alumel and chromel, respectively)

Thermocouple	d_a	d_c	d_a/d_c	$\Delta T_a/\Delta T_c$
OMEGA 24AWG Type-K TC	0.511 mm	0.511 mm	1	0.362
Balanced Thermocouple: K2	0.405 mm	0.511 mm	0.793	0.917

It can be seen from Table 3.2.2 that thermocouple K2 has greatly improved the imbalance associated with the joule heating of the leads. If a 24AWG chromel wire and an alumel wire with a diameter of 0.396mm (0.01559 in.) were welded together, the temperature balance would be unity. This specific diameter is not available from thermocouple manufacturers and therefore was not used.

3.3 Data Reduction Procedure

Figure 3.3.1 presents a typical dimensionless temperature decay response generated from data collected from an LCSR test. A MATLAB program was used to perform the necessary data reduction and calculate the parameters of interest, namely, τ_0, λ, τ_{max}, and t_{cr}. It must be noted that the actual test data is presented in Figure 3.3.1. However, the data was filtered, using a built-

in MATLAB command, and used to calculate the parameters of interest. The proceeding data reduction method was utilized to characterize the thermocouple response.

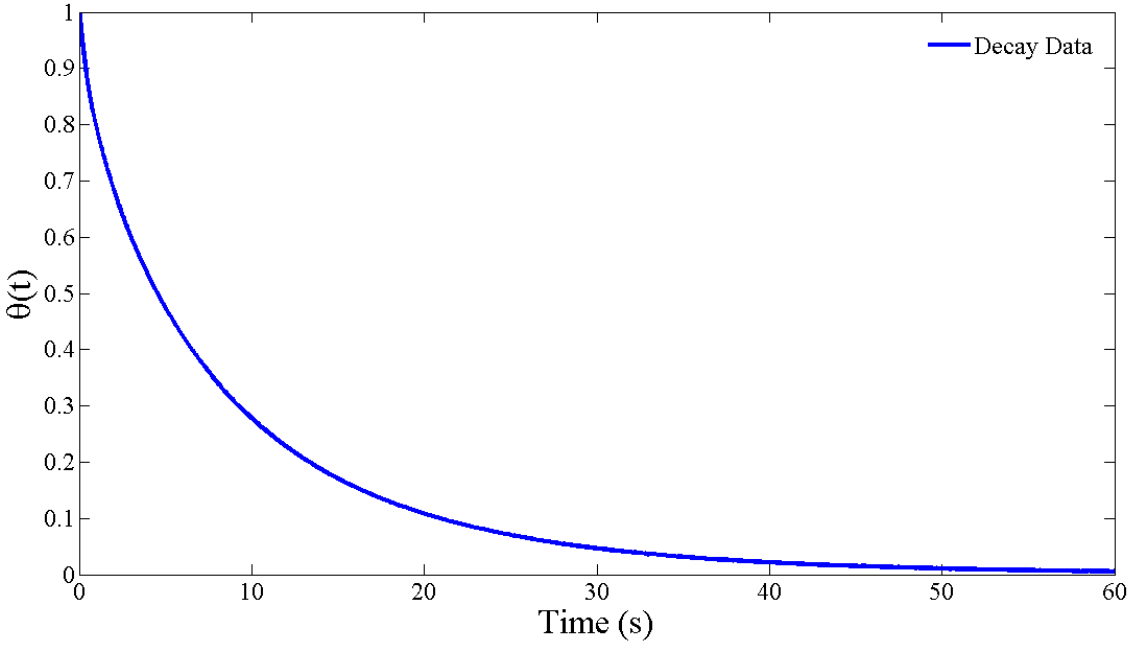

Figure 3.3.1 An example of a typical plot of dimensionless LCSR decay data.

For constant ambient temperature, recall the exact solution for the thermocouple model (Eq. 2.1.12) as

$$\theta_{TC}(t) = \exp\left\{\frac{1}{2\lambda^2}\left[\tau_0 \ln\left(\tau_0 + 2\lambda\sqrt{t}\right) - \tau_0 \ln\left(\tau_0\right) - 2\lambda\sqrt{t}\right]\right\}, \qquad t \geq 0, \tag{3.3.1}$$

where

$$\theta_{TC}(t) = \frac{T_{TC}(t) - T_\infty}{T_{TC}(0) - T_\infty} \tag{3.3.2}$$

Taking the natural log of both sides of Eq. (3.1.1) yields

$$\ln\left(\theta_{TC}(t)\right) = \frac{1}{2\lambda^2}\left[\tau_0 \ln\left(\tau_0 + 2\lambda\sqrt{t}\right) - \tau_0 \ln\left(\tau_0\right) - 2\lambda\sqrt{t}\right] \tag{3.3.3}$$

After some manipulation, the above equation may be rewritten as

$$\ln\left(\theta_{TC}(t)\right) = \frac{\tau_0}{2\lambda^2}\left[\ln\left(1+\frac{2\lambda}{\tau_0}\sqrt{t}\right)-\frac{2\lambda}{\tau_0}\sqrt{t}\right] \tag{3.3.4}$$

It is convenient to define $\frac{\tau_0}{2\lambda^2}$ and $\frac{2\lambda}{\tau_0}$ as

$$a = \frac{\tau_0}{2\lambda^2} \tag{3.3.5}$$

$$b = \frac{2\lambda}{\tau_0} \tag{3.3.6}$$

Substituting *a* and *b* in Eq. (3.3.4) and rearranging yields

$$a = \frac{\ln\left(\theta_{TC}(t)\right)}{\ln\left(1+b\sqrt{t}\right)-b\sqrt{t}} \tag{3.3.7}$$

In order to satisfy this model, values for *a* and *b* must be obtained by analyzing dimensionless LCSR decay data collected from a thermocouple. This is done in an iterative fashion by substituting various *b* values into Eq. (3.3.7) for the time period of $t_1 \leq t \leq t_2$, where $\theta_{TC}(t_2) = 0.368$. In this analysis, $t_1 = 0$. For this given range of time and a given value of *b*, an array of *a* values was determined. The mean (M_a) and standard deviation (σ_a) of this array of *a* values were calculated. The optimal *b* value will be that which minimizes the ratio of standard deviation to the mean of the *a* array, i.e., when σ_a/M_a is minimized. Once the optimal *b* value is determined, the optimal *a* value is the mean of that particular *a* array. Figures 3.3.2 and 3.3.3 are graphical representations of the described calculation procedure. The figures show that for this data set $b_{opt} = 1.275\ s^{-1/2}$ and $a_{opt} = 0.499$, which corresponds to $\tau_0 = 2.51s$ and $\lambda = 1.60\ s^{1/2}$.

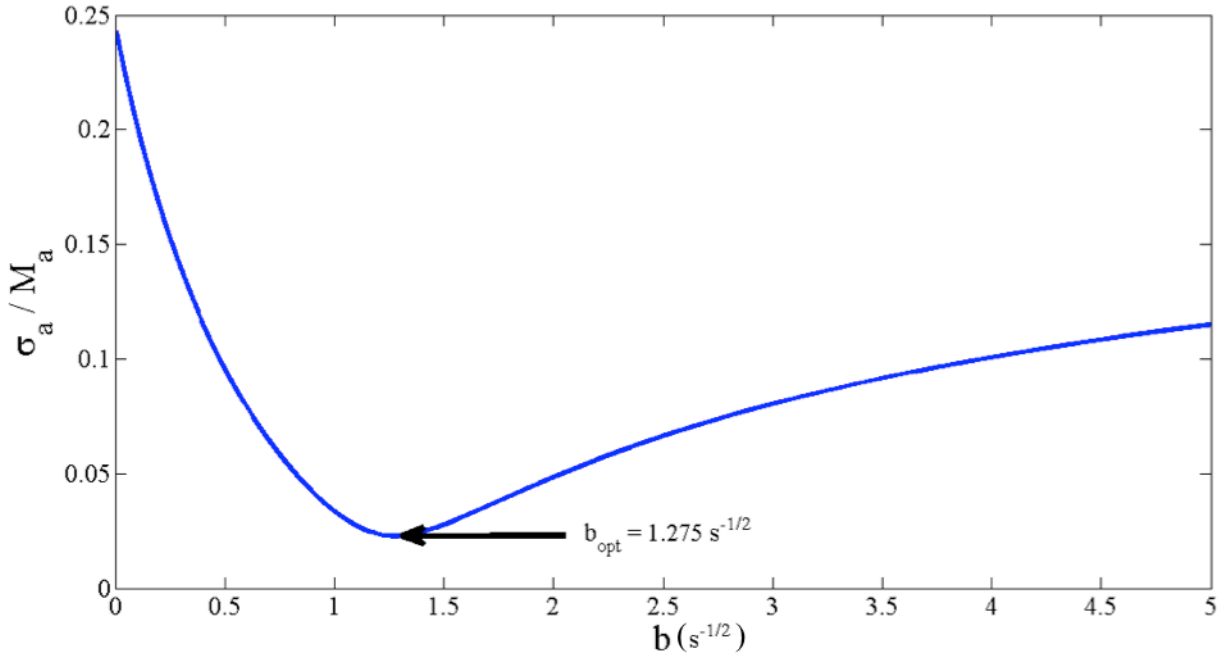

Figure 3.3.2 An example plot for the ratio of the dimensionless standard deviation to the mean of the *a* array for various values of *b*.

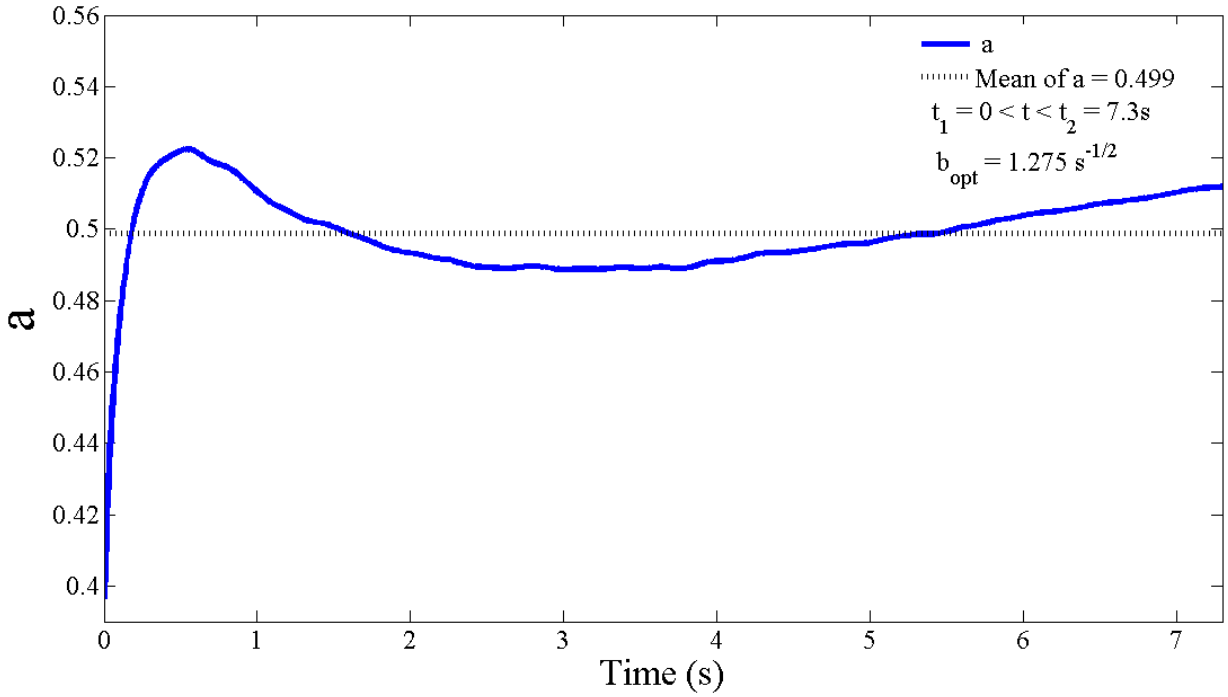

Figure 3.3.3 An example plot of the *a* array for the optimal value of $b = 1.275\ s^{-1/2}$ for the time range: $t_1 < t < t_2$.

Equation (3.3.4) should be valid up to $t \leq t_{cr}$. A plot of the left hand side and right hand side of Eq. (3.3.4) versus time can be used to obtain an estimate for t_{cr} as shown in Figure 3.3.4.

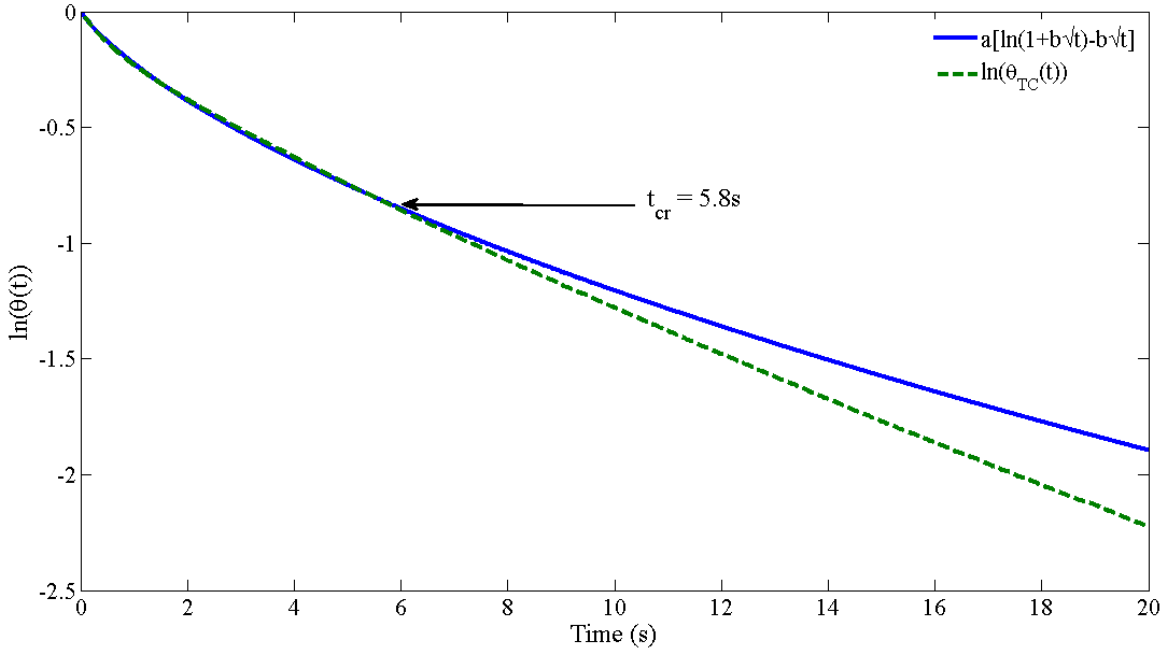

Figure 3.3.4 Natural log plot of the dimensionless LCSR decay data along with the model utilizing the values obtained for τ_0 and λ.

For this data set, Eq. (3.3.4) is valid up to t_{cr} = 5.8s. Finally, the last parameter of interest is τ_{max} and may be calculated by substituting τ_0, λ, and t_{cr} into Eq. (2.1.11):

$$\tau_{\max} = \tau_0 + 2\lambda\sqrt{t_{cr}} \tag{3.3.8}$$

For this data set, τ_{max} = 10.04s. At this point, all characterization parameters of interest have been calculated and may be applied to the full model for the response of the thermocouple:

$$\theta_{TC}(t) = \begin{cases} \exp\left\{\dfrac{1}{2\lambda^2}\left[\tau_0 \ln\left(\tau_0 + 2\lambda\sqrt{t}\right) - \tau_0 \ln(\tau_0) - 2\lambda\sqrt{t}\right]\right\}, & t \leq t_{cr} \\ \exp\left\{\dfrac{1}{2\lambda^2}\left[\tau_0 \ln\left(\tau_0 + 2\lambda\sqrt{t_{cr}}\right) - \tau_0 \ln(\tau_0) - 2\lambda\sqrt{t_{cr}} - 2\lambda^2 \dfrac{t - t_{cr}}{\tau_{\max}}\right]\right\}, & t > t_{cr} \end{cases} \tag{3.3.9}$$

Figure 3.3.5 presents a comparison of the experimental decay data with the full model using the calculated response parameters. This comparison clearly demonstrates that the balanced-leads TC test data conforms to the underlying physics and assumptions used to obtain the analytical model.

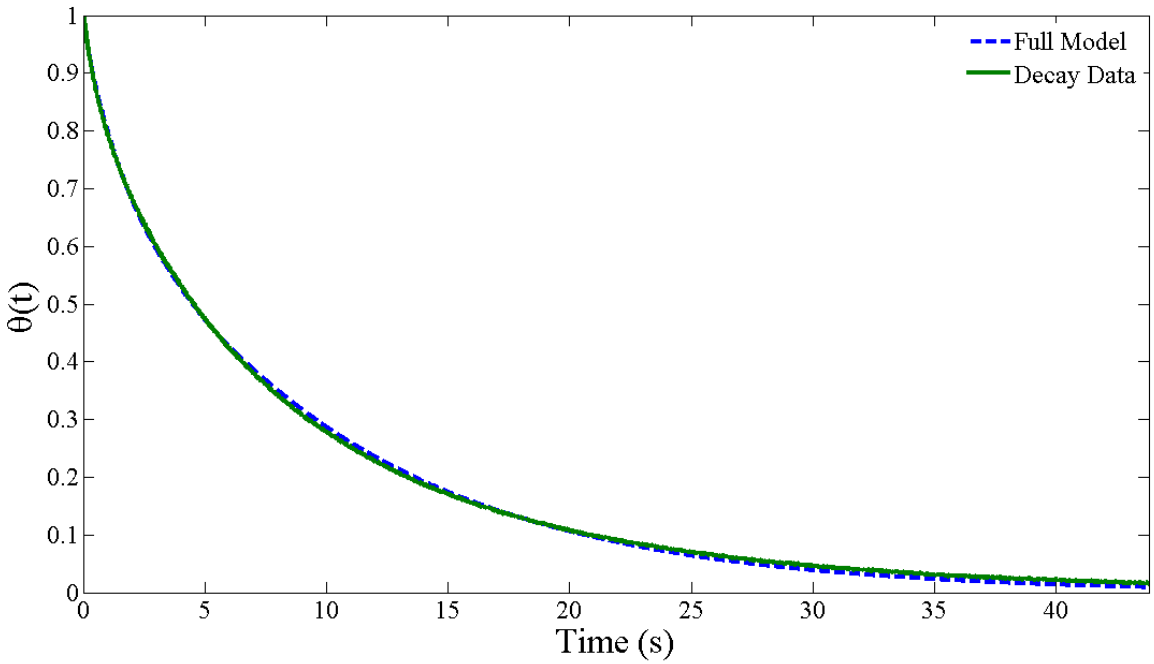

Figure 3.3.5 Comparison of the dimensionless decay data with the full model evaluated for τ_0 = 2.51s, λ = 1.60 $s^{1/2}$, t_{cr} = 5.8s, and τ_{max} = 10.04s

CHAPTER 4: RESULTS

4.1 Limitations of Conventional First-Order Model Analysis

For industrial applications, thermocouples are often analyzed as first-order systems. This is not always a valid assumption. This point will be demonstrated by presenting and discussing the LCSR test data of a standard 24AWG Type-K TC and of a balanced-leads thermocouple (K2). Both thermocouples were installed in air and subjected to an air velocity of 110 cm/s with their lead wires covered with insulation. The heating duration and current limitation for both tests were 5 seconds and 2.0 A, respectively. The decay data of the standard 24AWG TC is presented in Figure 4.1.1, and the decay data of the K2 TC is presented in Figure 4.1.2.

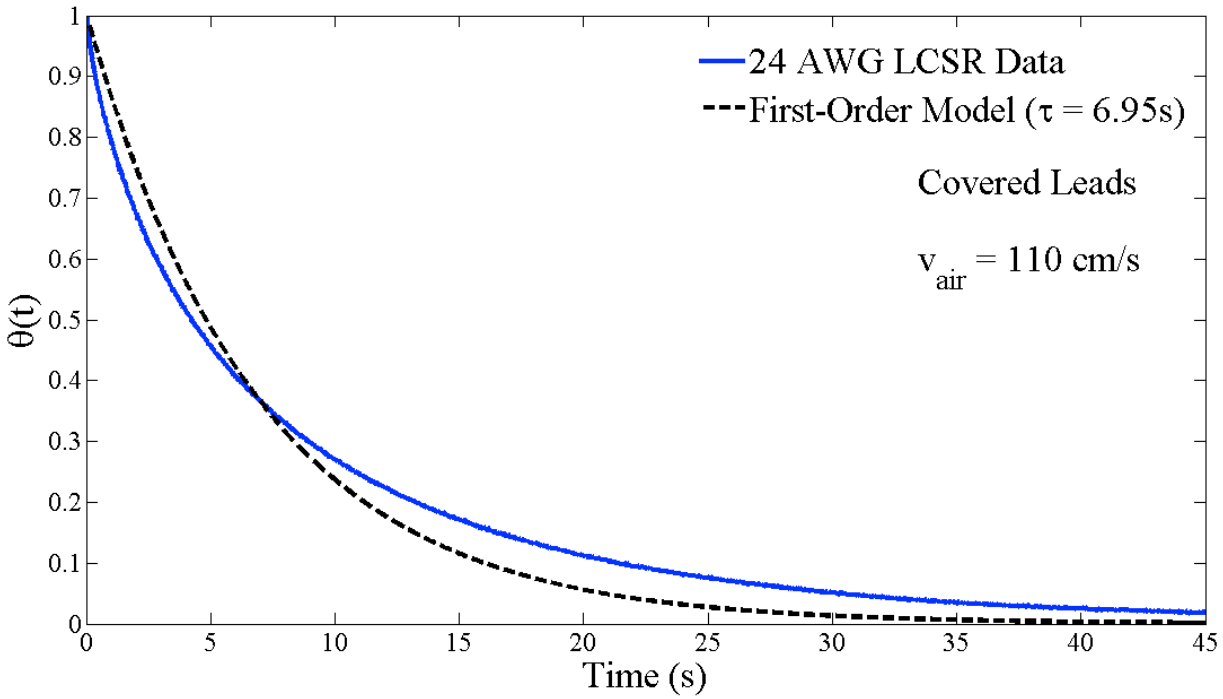

Figure 4.1.1 Comparison of the LCSR response data from a standard 24AWG Type-K TC with its leads covered with insulation with a first-order model.

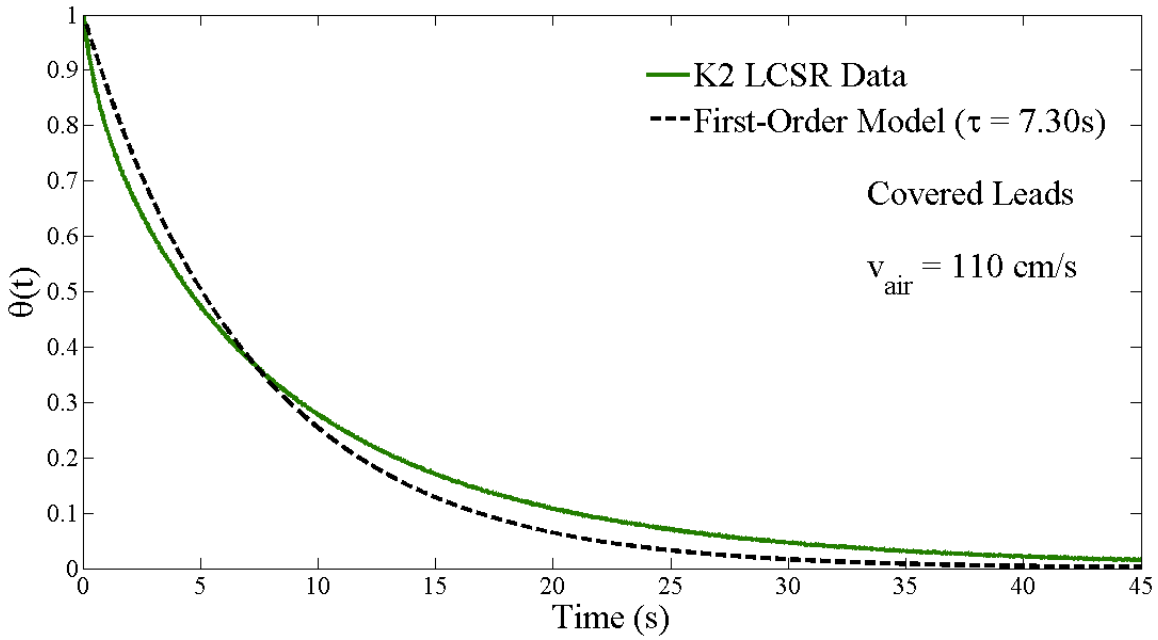

Figure 4.1.2 Comparison of the LCSR response data from the K2 TC with its leads covered with insulation with a first-order model.

For both data sets, the plots show that a first-order model may not be applied to a thermocouple under such conditions. The first-order model over predicts the response of the thermocouple for $0 < t < \tau$ and under predicts the response for $t > \tau$, where τ by definition is the time at which the dimensionless temperature decay is equal to 0.368. For each data set, the difference between the decay data and its corresponding first-order model is calculated and denoted as dimensionless residual, $\Re_f$. The calculated residuals are compared in Figure 4.1.3.

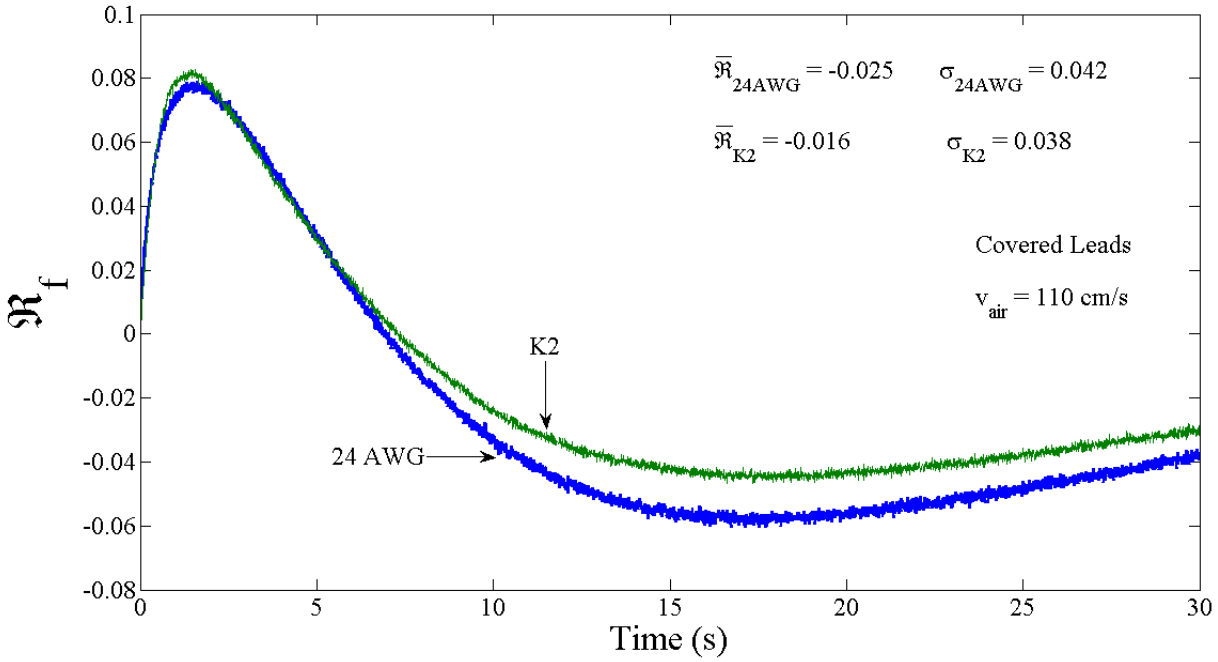

Figure 4.1.3 Comparison of the dimensionless residual plots of the standard 24AWG TC and the K2 TC test data. The residual represents the difference between the covered leads test data and the first-order model.

Although the residual of K2 is less than the standard 24 AWG TC, neither thermocouple exhibits first-order behavior under these conditions. The first-order model for a lumped system does not account for axial conduction from the leads. When the leads of the thermocouple are covered with insulation, there is a significant temperature difference between the leads and the bead during LCSR heating. As the bead cools rapidly, the heat from the leads transfers to the bead and slows down the decay. Therefore, a first-order approach for analysis cannot be applied to a thermocouple whose leads are covered with insulation.

However, if the leads of the thermocouple are exposed, then the decay response can be modeled as a first-order system with improved accuracy. In this case, the temperature difference between the exposed part of the leads and the bead is reduced, thus reducing the axial conduction lead effect (smaller λ). Clearly, as the length of the exposed part of the leads increases, λ approaches zero. This point will be demonstrated by presenting and discussing the LCSR test data of a

standard 24AWG Type-K TC and of the K2 TC. Both thermocouples were installed in air and subjected to an air velocity of 110 cm/s with their lead wires exposed approximately 12 mm. The heating duration and current limitation for both tests were 5 seconds and 2.0 A, respectively. The decay data of the standard 24AWG Type-K TC is presented in Figure 4.1.4, and the decay data of the K2 TC is presented in Figure 4.1.5.

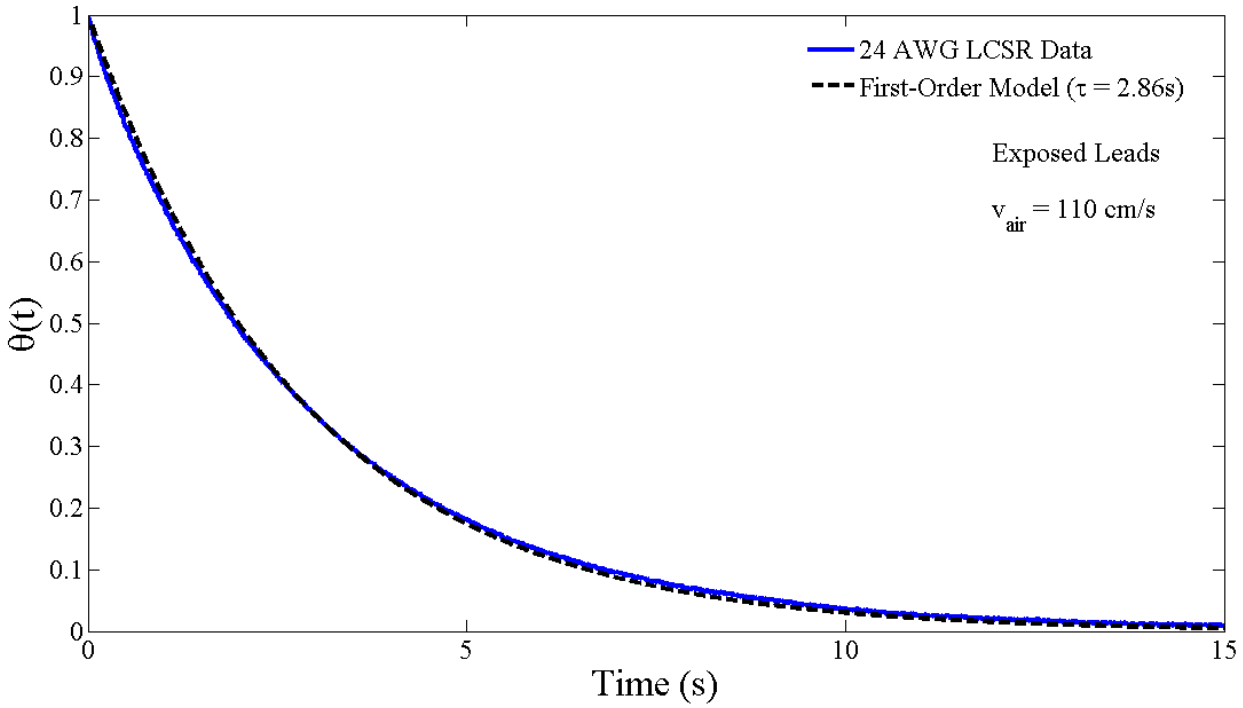

Figure 4.1.4 Comparison of the LCSR dimensionless response data from a standard 24AWG Type-K TC with its leads exposed with a first-order model.

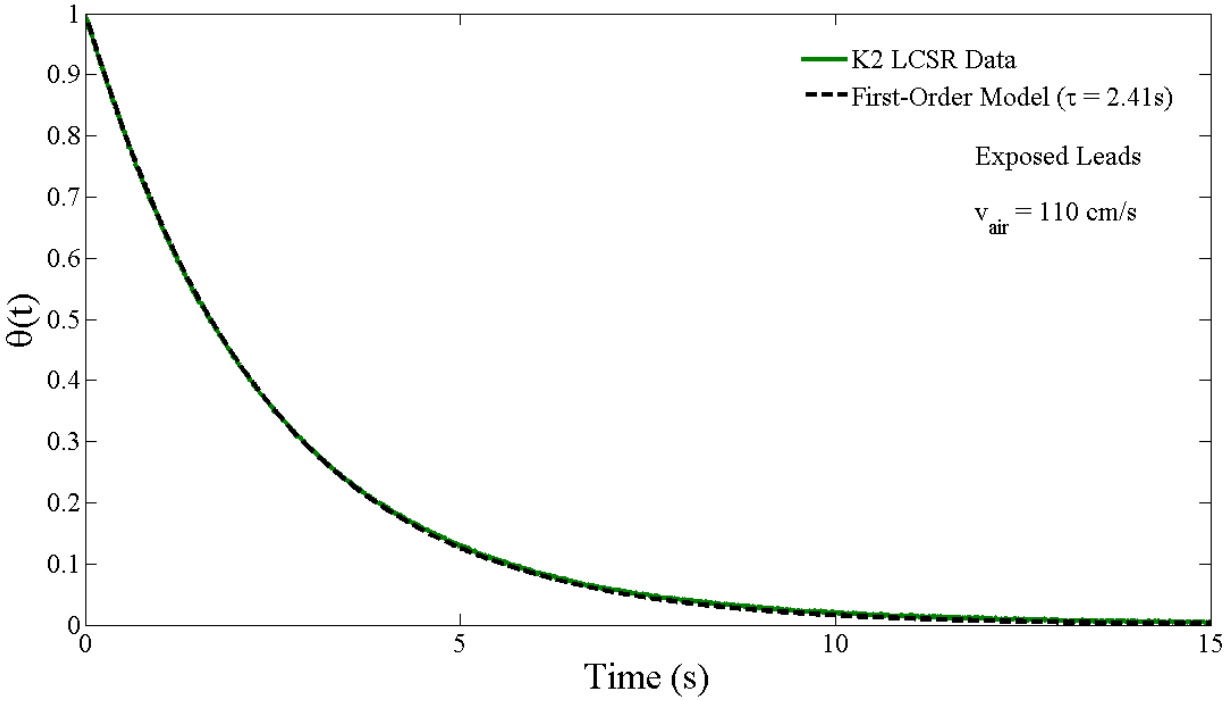

Figure 4.1.5 Comparison of the LCSR dimensionless response data from the K2 TC with its leads exposed with a first-order model.

For both data sets, the plots show that the first-order model provides a very good approximation of the test data. Figure 4.1.4 shows that the decay data of the standard 24AWG TC exhibits a weak axial conduction effect (slight over prediction at early decay time and slight under prediction at larger decay time). However, for the balanced-leads TC, Figure 4.1.5, the magnitude of over prediction and under prediction during the decay period is reduced which suggests that the axial conduction parameter is approximately zero ($\lambda \approx 0$). It can be stated that both data sets conform relatively well to the physics of a first-order model. It is interesting to note that the time constant of the standard thermocouple (τ = 2.86s) is larger than the time constant of the balanced-leads thermocouple (τ = 2.41s). This is due to the fact that the standard 24 AWG TC bead is larger than the K2 TC bead (under identical test conditions, the larger TC bead will have a larger time constant). However, for the covered leads case, the first-order model approximation resulted in a time constant of 6.95s for the standard thermocouple, which is smaller than the time constant of 7.3s for the K2 thermocouple. This is contrary to the relative magnitudes obtained from the exposed test case. Recall that the covered leads test data sets do

not conform to first-order model physics. Therefore, the calculated "time constant" values merely represent the time at which the dimensionless temperature decay data equals 0.368.

For each data set, the difference between the decay data and its corresponding first-order model is calculated and denoted as the dimensionless residual, $\Re_f$. The calculated residuals are compared in Figure 4.1.6. In the early decay period (t < 3s), the residual for the K2 TC is much smaller than the residual for the 24 AWG TC. This is the evidence that the attempt to construct a balanced-leads thermocouple has resulted in a smaller temperature difference between the K2 TC bead and its leads. This is to be expected. The assumption for a lumped system is that the system is at a uniform temperature at the beginning of the response. Recall from Section 3.2 (Table 3.2.1) that TC K2's leads and bead experience almost the same temperature rise while the 24AWG TC's chromel lead experiences more than 2.7 times higher temperature rise than the alumel lead.

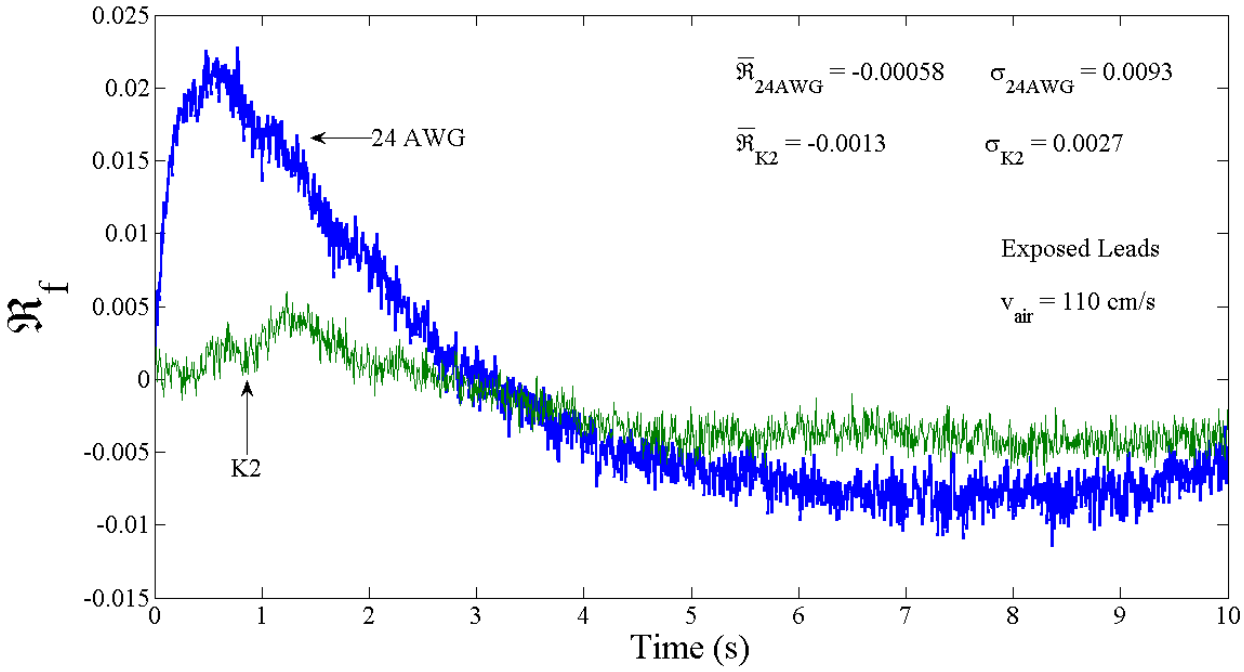

Figure 4.1.6 Comparison of the residual plots of the standard 24AWG TC and the K2 TC test data. The residual represents the difference between the exposed leads test data and the first-order model.

4.2 Full Model Data Characterization

The full model developed for the purpose of characterizing in-situ thermocouples may be applied to a thermocouple regardless of the exposure of its lead wires. Figure 4.2.1 compares the covered leads 24 AWG test data with the full model. The response characterization parameters of this data set are: τ_0 = 2.69s, τ_{max} = 9.54s, λ = 1.40 $s^{1/2}$, t_{cr} = 6.00s. To demonstrate the axial conduction lead effect, the TC decay as predicted by the full model for τ_0 = 2.69s and λ = 0 (which reduces to a first-order model) is also plotted in Figure 4.2.1. Figure 4.2.2 compares the covered leads K2 test data with the full model. The response characterization parameters of this data set are: τ_0 = 2.47s, τ_{max} = 9.67s, λ = 1.57 $s^{1/2}$, t_{cr} = 5.70s. To demonstrate the axial conduction lead effect for the K2 TC, the TC decay as predicted by the full model for τ_0 = 2.47s and λ = 0 (which reduces to a first-order model) is also plotted in Figure 4.2.2. Again, it is observed that the calculated τ_0 value for the standard 24 AWG TC (2.69s) is larger than the calculated that of the K2 TC (2.47s). This further reinforces the fact that τ_0 is an intrinsic property of the thermocouple.

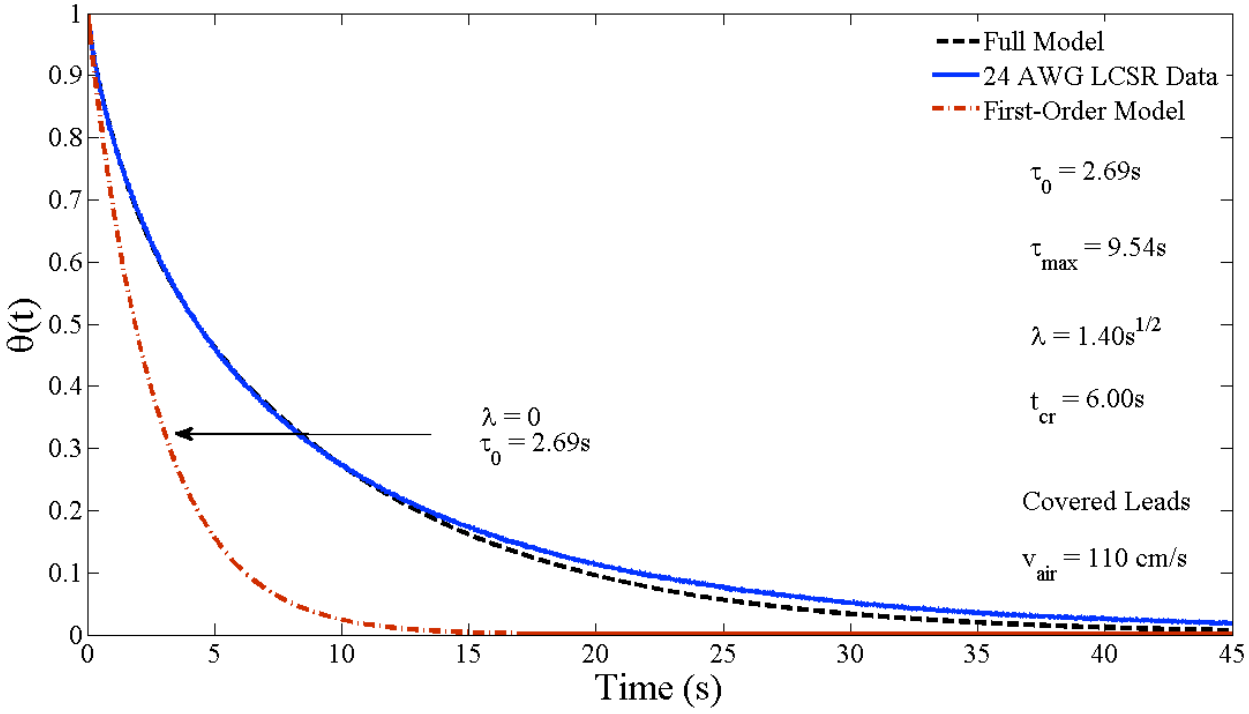

Figure 4.2.1 Comparison of the covered leads LCSR dimensionless response data for the 24 AWG TC with the full model and the first-order model for τ_0 = 2.69s.

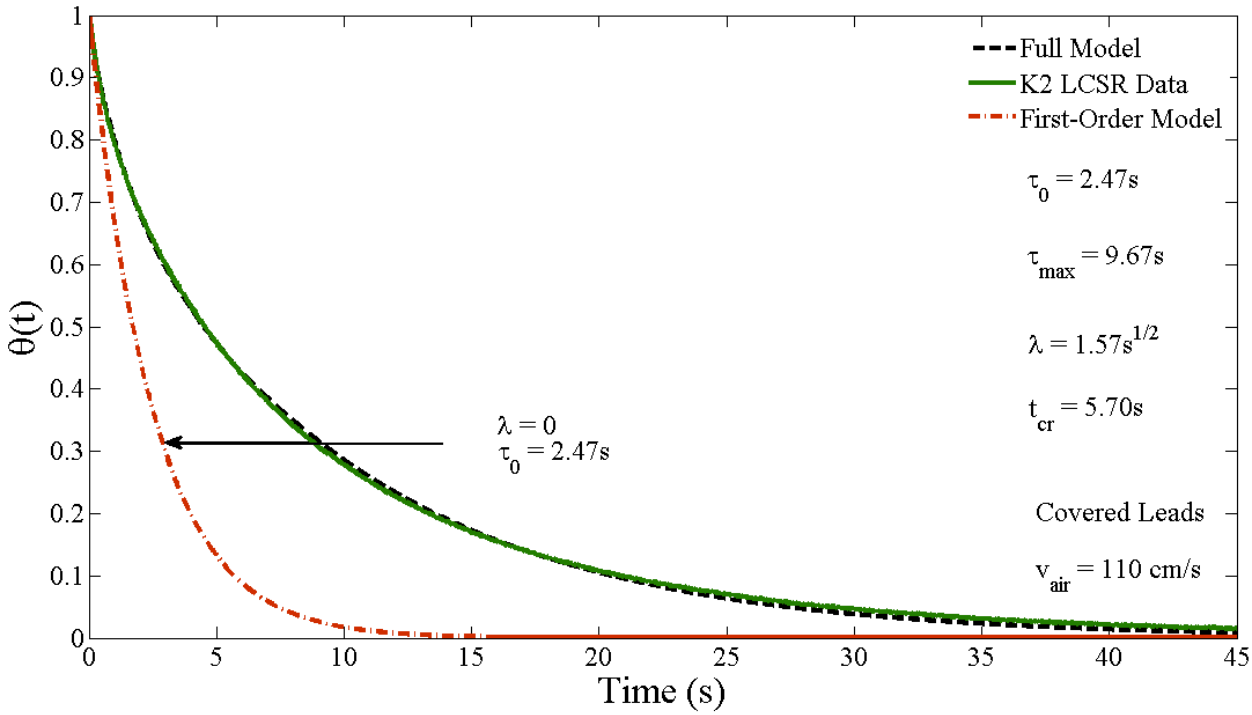

Figure 4.2.2 Comparison of the covered leads LCSR dimensionless response data for the K2 TC with the full model and the first-order model for $\tau_0 = 2.47$s.

For each data set, the difference between the decay data and its corresponding full model is calculated and denoted as residual, $\Re$. The calculated residuals are compared in Figure 4.2.3. The magnitudes of the mean of the residual and standard deviation of the residual for the K2 TC are slightly less than those for the standard 24 AWG TC.

Figure 4.2.4 compares the exposed leads 24 AWG test data with the full model. The response characterization parameters of this data set are: $\tau_0 = 2.32$s, $\tau_{max} = 3.10$s, $\lambda = 0.27$ s$^{1/2}$, $t_{cr} = 2.00$s. To demonstrate the axial conduction lead effect, the TC decay as predicted by the full model for $\tau_0 = 2.32$s and $\lambda = 0$ (which reduces to a first-order model) is also plotted in Figure 4.2.4. In contrast to the covered leads case (Figure 4.2.1), the data set exhibits even better agreement with the full model. The axial conduction lead parameter for the exposed case ($\lambda = 0.27$ s$^{1/2}$) is significantly lower than that for the covered leads case ($\lambda = 1.40$ s$^{1/2}$).

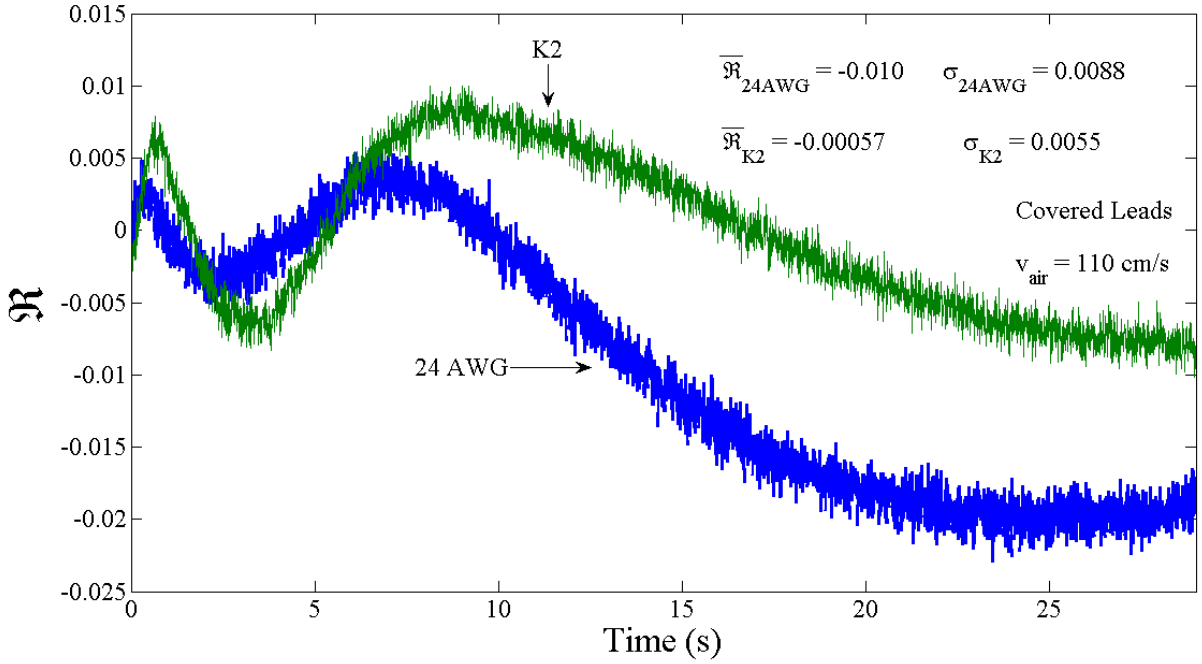

Figure 4.2.3 Comparison of the residual plots of the standard 24AWG TC and the K2 TC test data. The residual represents the difference between the covered leads test data and the full model.

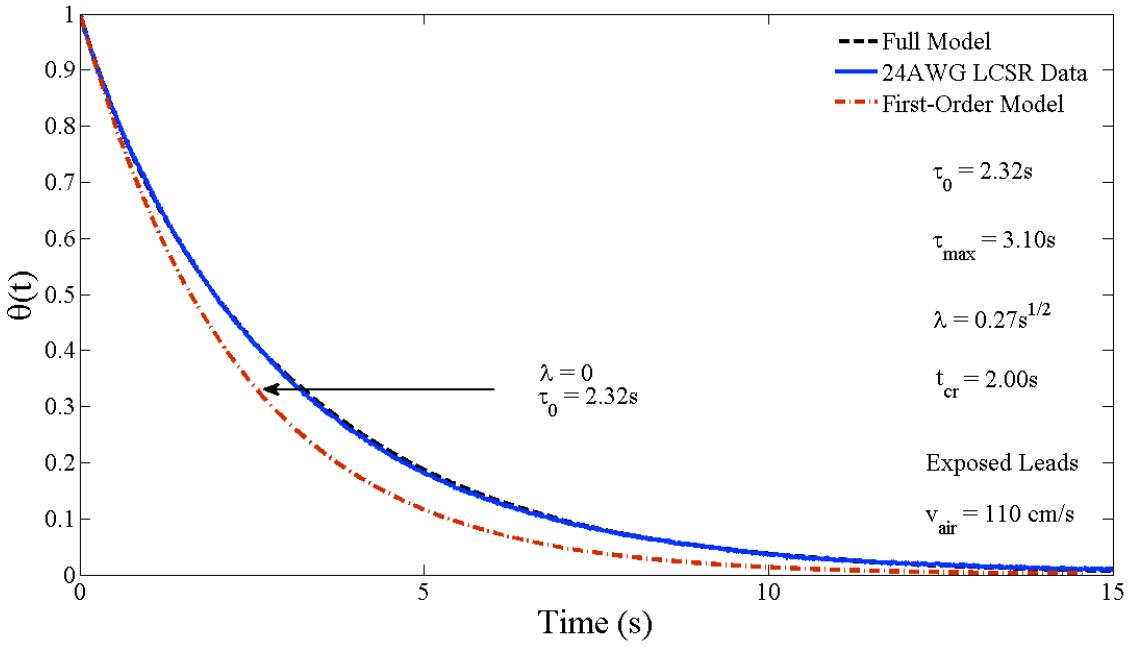

Figure 4.2.4 Comparison of the exposed leads LCSR dimensionless response data for the 24 AWG TC with the full model and the first-order model for $\tau_0 = 2.32s$.

Figure 4.2.5 compares the exposed leads K2 TC test data with the full model. The response characterization parameters of this data set are: $\tau_0 = 2.41$s, $\tau_{max} = 2.43$s, $\lambda = 0.01$ $s^{1/2}$, $t_{cr} = 4.00$s. To demonstrate the minimal axial conduction lead effect, the TC decay as predicted by the full model for $\tau_0 = 2.41$s and $\lambda = 0$ (which reduces to a first-order model) is also plotted in Figure 4.2.5. The data set exhibits excellent agreement with the full model. The axial conduction lead parameter for the exposed case ($\lambda = 0.01$ $s^{1/2}$) is significantly lower than that for the covered leads case ($\lambda = 1.57$ $s^{1/2}$).

It is significant to note that for the K2 thermocouple, the τ_0 value for the covered case ($\tau_0 = 2.47$s) is nearly the same as that for the exposed leads case ($\tau_0 = 2.41$s). This agreement is further evidence that for the balanced-leads thermocouple, the analysis of the LCSR test decay data via the full model yields an intrinsic parameter of the thermocouple system. However, for the 24 AWG thermocouple the τ_0 value for the covered case ($\tau_0 = 2.69$s) is different from the exposed leads case ($\tau_0 = 2.32$s), and the difference may not be attributed to data uncertainty.

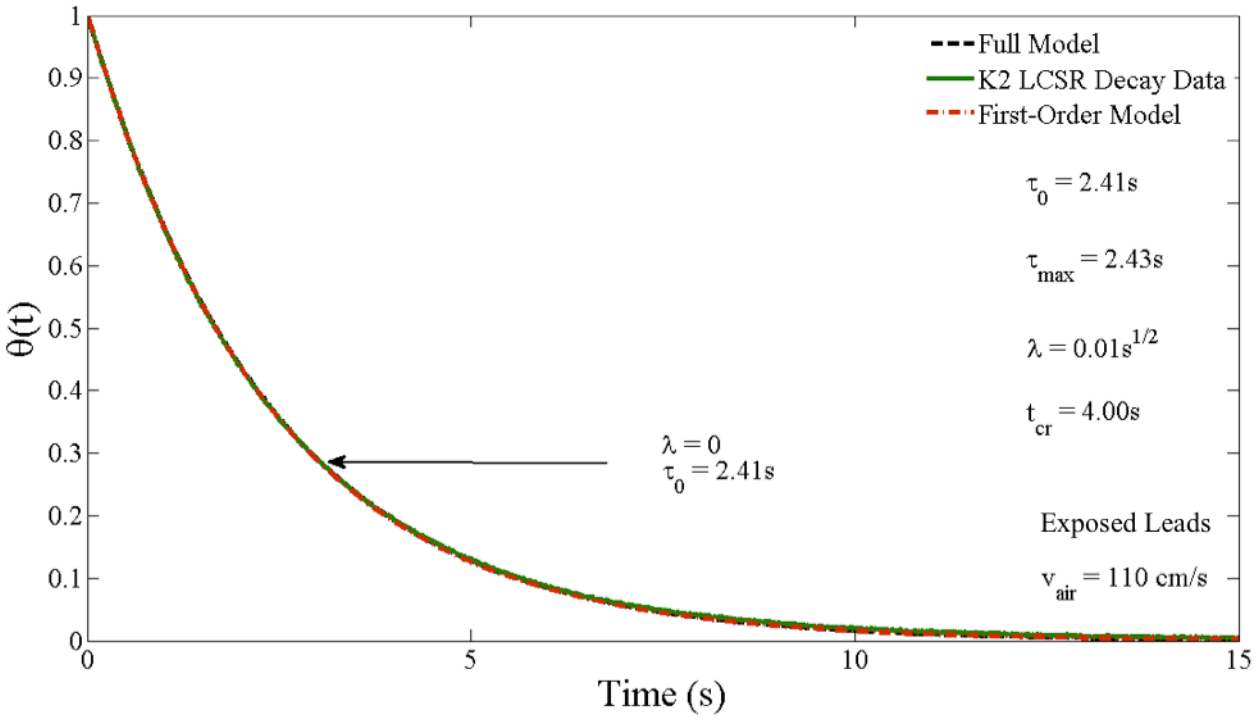

Figure 4.2.5 Comparison of the exposed leads LCSR dimensionless response data for the K2 TC with the full model and the first-order model for $\tau_0 = 2.41$s.

For each data set, the difference between the decay data and its corresponding full model is calculated and denoted as residual, $\Re$. The calculated residuals are compared in Figure 4.2.6. The magnitudes of the mean of the residual and standard deviation of the residual for the K2 TC are less than those for the standard 24 AWG TC.

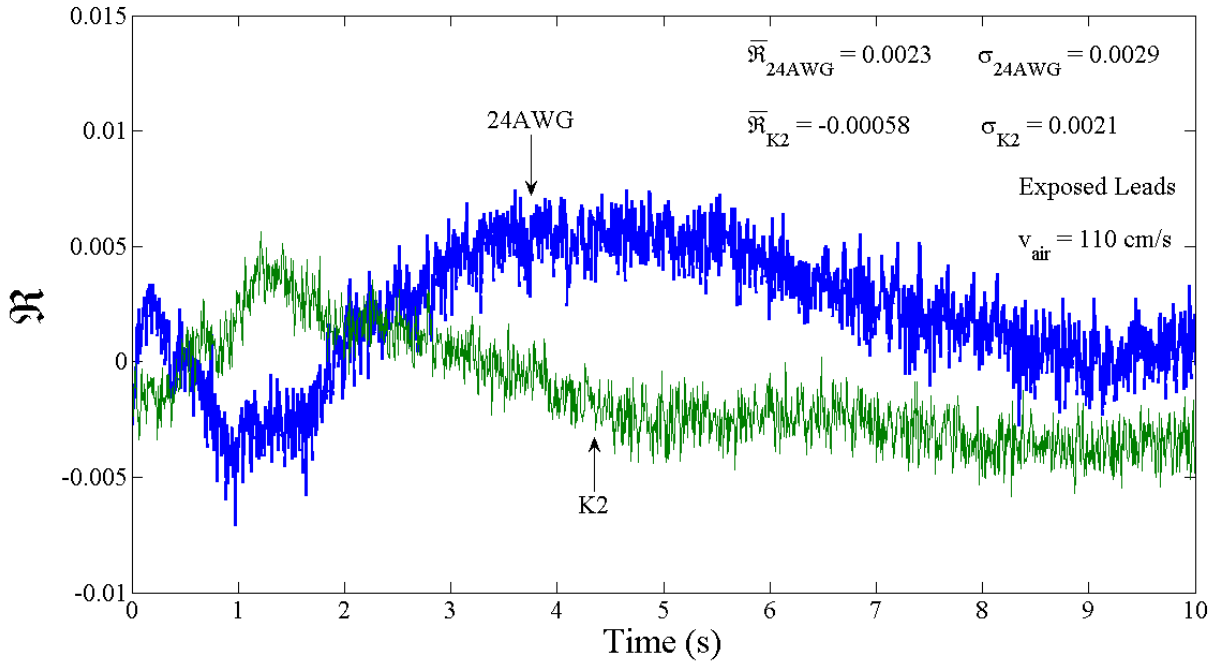

Figure 4.2.6 Comparison of the residual plots of the standard 24AWG TC and the K2 TC test data. The residual represents the difference between the exposed leads test data and the full model.

4.3 Fluid Velocity Calibration

LCSR tests were conducted on the K2 TC exposed to air flowing at velocities of 10 to 150 cm/s (instrumentation error for TSI VelociCalc 8345: 3% of reading or ±1.5 cm/s, whichever is greater) across the TC bead with its leads exposed by 3 mm. The data was sampled at 100 Hz and a gain of 32. The heating duration was 1 second at a current of 3 A. The zoomed in dimensionless temperature decay data is presented in Figure 4.3.1. A horizontal line at the dimensionless decay value of 0.368 is drawn in the figure to clearly show the intersection of that line with each set of decay data ($t = \tau$).

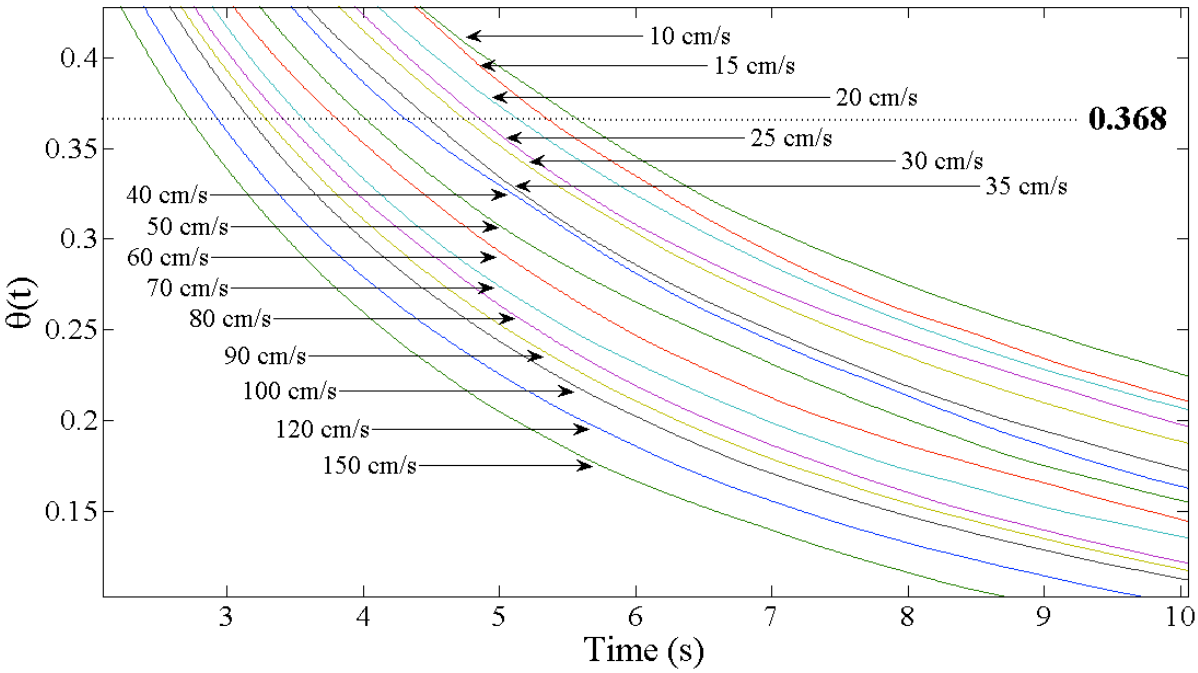

Figure 4.3.1 Zoomed in plot of dimensionless temperature decay data sets for various air velocities ranging from 10 cm/s to 150 cm/s with a line at θ(t) = 0.368.

The decay data clearly shows a very good sensitivity of the decay time constants to the measured air velocities. The measured time constant values can be converted to Nusselt numbers using the values of the bead diameter along with density and specific heat capacity of the bead. The bead diameter was measured to be D = 0.81 mm. The measured τ values were converted to convection heat transfer coefficient via

$$h = \frac{V_{TC}(\rho C)_{TC}}{\tau A_s} \tag{4.3.1}$$

where V_{TC} is the volume of the thermocouple bead and $(\rho C)_{TC}$ is the volume specific thermal capacitance of the TC bead. The weighted average scheme based on the lead diameter dimensions was used to calculate the volume specific thermal capacitance of the balanced-leads thermocouple bead. The calculated convection heat transfer coefficients were converted to Nusselt numbers ($Nu_D = hD/k$), and the measured air velocities were converted to Reynolds numbers ($Re_D = v_{air}D/\nu$). The thermophysical properties of air at T = 300K were used to perform

these calculations. Table 4.3.1 presents the experimental data converted to Nu_D and Re_D for air velocities ranging from 10 cm/s to 150 cm/s.

Table 4.3.1 Present data converted to Re_D, h, and Nu_D for air velocities of 10 cm/s to 150 cm/s (bead diameter = 0.81 mm).

Velocity (cm/s)	τ (s)	Re_D	h ($WK^{-1}m^{-2}$)	Nu_D
10	5.467	5.09	103.07	3.17
15	5.258	7.64	107.17	3.30
20	5.045	10.19	111.69	3.44
25	4.813	12.74	117.08	3.61
30	4.660	15.28	120.92	3.72
35	4.415	17.83	127.63	3.93
40	4.237	20.38	132.99	4.10
50	3.952	25.47	142.58	4.39
60	3.805	30.57	148.09	4.56
70	3.541	35.66	159.13	4.90
80	3.369	40.75	167.26	5.15
90	3.232	45.85	174.35	5.37
100	3.120	50.94	180.61	5.56
120	2.894	61.13	194.71	6.00
150	2.692	76.42	209.32	6.45

The experimental data was plotted along with the forced convection correlations for Pr = 0.71 and mixed convection estimation (that were presented in Section 1.2) as shown in Figure 4.3.2. Rayleigh number of 2.5 ($\Delta T_{TC} \approx 50°C$) was used to estimate the mixed convection values. It must be emphasized that the correlations are obtained from experimental data that is subject to uncertainty. More over, there is a deviation between any correlation and its corresponding data set. Numerical predictions also include some level of uncertainty analogous to experimental uncertainty. Clearly, the present data set is also subject to some level of uncertainty. A rigorous uncertainty analysis of the present data and quantification of the uncertainty of the correlations is not in the scope of this preliminary proof of concept work.

Considering that each entry plotted in Figure 4.3.2 is subject to some level of uncertainty, the agreement between the present data with the correlations is considered to be very good. These results re-enforce the validity of the assumptions made regarding LCSR for a balanced-leads thermocouple. It is demonstrated that one can conduct an LCSR test on a balanced-leads thermocouple in a fluid domain as a practical method for performing low velocity measurements on an in-situ sensor. However, in order to fully develop a dual-purpose thermocouple that is capable of measuring both temperature and fluid velocity, it is necessary to construct a thermocouple with a lead temperature ratio of unity and perform careful calibration tests on the thermocouple at various air velocities. This study validated a thermocouple model for a specially designed balanced-leads thermocouple using an established in-situ sensor characterization method that yields accurate positional temperature data as well as fluid velocity data.

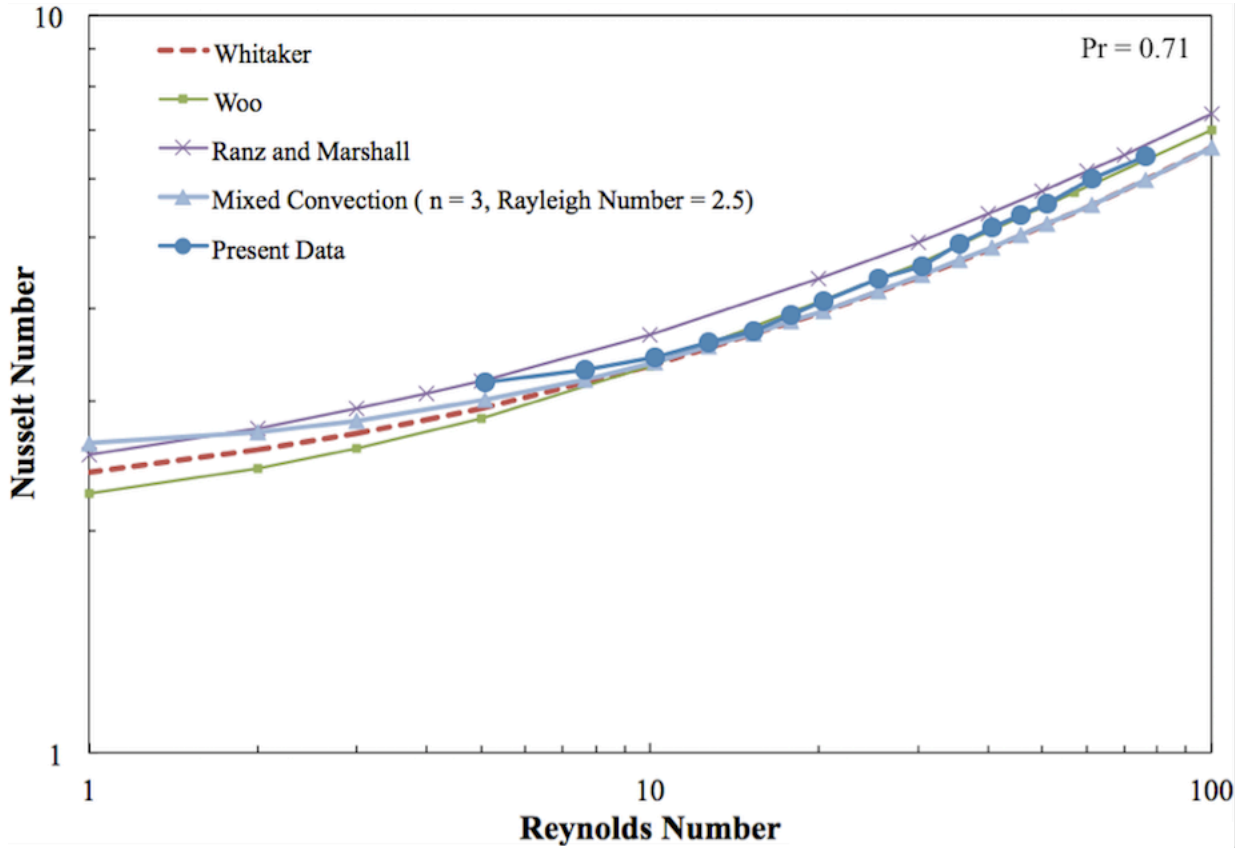

Figure 4.3.2 Comparison of present data converted to Nusselt numbers with forced convection correlations for Pr = 0.71 along with mixed convection estimation for n = 3, Ra_D = 2.5.

CHAPTER 5: CONCLUSIONS AND RECOMMENDATIONS

In this study, a specialized balanced-leads thermocouple was developed to perform in-situ thermal response characterization via the LCSR test method. Thermal response characterization of installed thermocouples is essential in order to obtain accurate positional temperature data in rapid transient applications. An analytical model is presented that fully describes the thermocouple system based on a first-principles approach to the heat transfer physics of the sensor. In conjunction with the LCSR test, the full model presented yields quantifiable characterization parameters useful for determining accurate positional temperature data. It is necessary to employ a balanced-leads thermocouple for this experimental procedure in order to ensure that the thermocouple bead and its leads are at the same initial temperature, when performing the LCSR test. If the installed thermocouple is in a fluid domain, it has been demonstrated that the LCSR test data may be calibrated against the fluid velocity. This finding was verified by comparison of the present experimental data with forced convection correlations obtained by previous researchers.

The next task to improve the work of this study is to construct a balanced-leads thermocouple with a lead temperature ratio of unity. This new balanced-leads thermocouple will more closely satisfy the assumptions made for applying the full model to the thermocouple system. For this study, the data obtained was compared with previous researchers' convection correlations to demonstrate a proof of concept. Lastly, the thermocouple sensor should be calibrated carefully over a wider velocity range before it can be implemented in an industrial application. This calibration procedure must be repeated for each individual thermocouple sensor to be installed. If these additional tasks are performed, a balanced-leads thermocouple characterized via the LCSR test method could become a valuable and versatile temperature-velocity probe for industrial processes.

REFERENCES

1. Carroll, R.M. and Shepard, R. L., (1977). *Measurement of the Transient Response of Thermocouples and Resistance Thermometers Using an In Situ Method*. Report ORNL/TM-4573, Oak Ridge National Laboratory, USA.

2. Yue, Z. and Malmstöm, T. G. (1998). A Simple Method for Low-Speed Hot-Wire Anemometer Calibration, *Meas. Sci. Technol*, 9, 1506-1510.

3. Christman, Paul J. and Podzimek, Josef., (1981) Hot-wire Anemometer Behavior in Low Velocity Air Flow, *J. Phys. E: Sci. Instrum*, 14, 46.

4. Whitaker, S., (1972). Forced Convection Heat Transfer Calculations for Flow in Pipes, Past Flat Plates, Single Cylinders, Single Spheres, and for Flow in Packed Beds and Tube Bundles, *AIChE J.,* 18, 361.

5. Ranz, W., and Marshall, W., (1952). Evaporation from Drops. *Chem. Eng. Prog.,* 48, 141.

6. Woo, Sun-Wai, (1971). *Simultaneous Free and Forced Convection Around Submerged Cylinders and Spheres*. Ph.D. Dissertation, McMaster University, Hamilton, Ontario, Canada.

7. Churchill, S.W., "Free Convection Around Immersed Bodies," in G. F. Hewitt, Exec. Ed., *Heat Exchanger Design Handbook,* Section 2.5.7, Begell House, New York, 2002.

8. Churchill, S. W., and Ozoe, H., (1973). Correlations for Laminar Forced Convection with Uniform Heating in Flow over a late and in Developing and Fully Developed Flows in a Tube. *J. Heat Transfer, Trans*. ASME, 95C, 78.

9. Frankel, J., (2007), Regularization of inverse heat conduction by combination of rate sensor analysis and analytical continuation, *Journal of Engineering Mathematics,* 57(2), pp. 181-198.

10. Elkins, B. S., (2011). *Challenges for the Accurate Determination of the Surface Thermal Condition via In-Depth Sensor Data.* Ph.D. Dissertation, University of Tennessee, Knoxville, TN, USA.

APPENDIX

A.1 LAPLACE TRANSFORM OF EQUATION (2.1.10)

Transform of Eq. (2.1.10) to form exact solution Eq. (2.1.12):

$$\left(\tau_0 + 2\lambda\sqrt{t}\right)\dot{T}_{TC}(t) + T_{TC}(t) \approx T_\infty(t) \tag{A.1}$$

This can be rewritten as

$$-T_\infty + T_{TC}(t) + \left(\tau_0 + 2\lambda\sqrt{t}\right)\dot{T}_{TC}(t) = 0 \tag{A.2}$$

Let $R(t,T_{TC}) = T_{TC}(t)-T_\infty$, $S(t,T_{TC}) = \tau_0-2\lambda\sqrt{t}$. Find an integrating factor, $\mu(t)$ such that

$$\mu(t)R(t,T_{TC}) + \mu(t)\dot{T}_{TC}(t)S(t,T_{TC}) = 0 \tag{A.3}$$

is exact. Taking partial derivatives with respect to temperature and time, Eq. (A.3) is rewritten as

$$\frac{\delta}{\delta T}\left(\mu(t)R(t,T_{TC})\right) = \frac{\delta}{\delta t}\left(\mu(t)S(t,T_{TC})\right) \tag{A.4}$$

Solving in terms of the integrating factor gives

$$\mu(t) = \frac{d\mu(t)}{\delta t}\left(\tau_0 + 2\lambda\sqrt{t}\right) + \frac{\lambda\mu(t)}{\sqrt{t}} \tag{A.5}$$

Which may be rearranged as

$$\frac{\dfrac{d\mu(t)}{\delta t}}{\mu(t)} = \frac{-\dfrac{\lambda}{\sqrt{t}} + 1}{\tau_0 + 2\lambda\sqrt{t}} \tag{A.6}$$

Taking the natural log of Eq. (A.6) and rearranging once again

$$\ln\left(\mu(t)\right) = \frac{\sqrt{t}}{\lambda} + \frac{(-\tau_0 - 2\lambda^2)\ln\left(\tau_0 + 2\lambda\sqrt{t}\right)}{2\lambda^2} \tag{A.7}$$

Finally, the integrating factor is expressed as

$$\mu(t) = e^{\frac{\sqrt{t}}{\lambda}}\left(\tau_0 + 2\lambda\sqrt{t}\right)^{\frac{-\tau_0}{2\lambda^2}-1} \tag{A.8}$$

Multiply both sides of Eq. (A.2) by $\mu(t)$ to obtain

$$e^{\frac{\sqrt{t}}{\lambda}}\left(-T_\infty + T_{TC}(t)\right)\left(\tau_0 + 2\lambda\sqrt{t}\right)^{\frac{-\tau_0}{2\lambda^2}-1} + \frac{e^{\frac{\sqrt{t}}{\lambda}}\dot{T}_{TC}(t)}{\left(\tau_0 + 2\lambda\sqrt{t}\right)^{\frac{\tau_0}{2\lambda^2}}} = 0 \tag{A.9}$$

Let $P(t,T_{TC})$ and $Q(t,T_{TC})$ be expressed as

$$P(t,T_{TC}) = (T_{TC}(t) - T_\infty)e^{\frac{\sqrt{t}}{\lambda}}\left(\tau_0 + 2\lambda\sqrt{t}\right)^{\frac{-\tau_0}{2\lambda^2}-1}, \qquad Q(t,T_{TC}) = \frac{e^{\frac{\sqrt{t}}{\lambda}}}{\left(\tau_0 + 2\lambda\sqrt{t}\right)^{\frac{\tau_0}{2\lambda^2}}} \tag{A.10}$$

Define $f(t,T_{TC})$ such that

$$\frac{\partial f(t,T_{TC})}{\partial t} = P(t,T_{TC}), \qquad \frac{\partial f(t,T_{TC})}{\partial T_{TC}} = Q(t,T_{TC}) \tag{A.11}$$

The solution will be given by $f(t,T_{TC}) = c_1$.

Integrate $P(t,T_{TC})$ to determine $f(t,T_{TC})$

$$\int e^{\frac{\sqrt{t}}{\lambda}}\left(-T_\infty + T_{TC}(t)\right)\left(\tau_0 + 2\lambda\sqrt{t}\right)^{\frac{-\tau_0}{2\lambda^2}-1} dt = \frac{e^{\frac{\sqrt{t}}{\lambda}}\left(-T_\infty + T_{TC}(t)\right)}{\left(\tau_0 + 2\lambda\sqrt{t}\right)^{\frac{\tau_0}{2\lambda^2}}} + g(T_{TC}) \tag{A.12}$$

Where $g(T_{TC})$ is some arbitrary function of T_{TC}.

$$\frac{\partial f(t,T_{TC})}{\partial T_{TC}} = \frac{\partial}{\partial T_{TC}}\left(\frac{e^{\frac{\sqrt{t}}{\lambda}}\left(-T_\infty + T_{TC}(t)\right)}{\left(\tau_0 + 2\lambda\sqrt{t}\right)^{\frac{\tau_0}{2\lambda^2}}} + g(T_{TC})\right) = \frac{e^{\frac{\sqrt{t}}{\lambda}}}{\left(\tau_0 + 2\lambda\sqrt{t}\right)^{\frac{\tau_0}{2\lambda^2}}} + \frac{dg(T_{TC})}{dT_{TC}} = Q(t,T_{TC}) \tag{A.13}$$

Substitution for $Q(t,T_{TC})$ yields

$$\frac{dg(T_{TC})}{dT_{TC}} = 0, \qquad g(T_{TC}) = 0 \tag{A.14}$$

$f(t,T_{TC})$ may now be written as

$$f(t,T_{TC}) = \frac{e^{\frac{\sqrt{t}}{\lambda}}\left(-T_\infty + T_{TC}(t)\right)}{\left(\tau_0 + 2\lambda\sqrt{t}\right)^{\frac{\tau_0}{2\lambda^2}}} = c_1 \tag{A.15}$$

Solving $f(t,T_{TC})$ in terms of T_{TC}

$$T_{TC}(t) = T_\infty + c_1 \frac{\left(\tau_0 + 2\lambda\sqrt{t}\right)^{\frac{\tau_0}{2\lambda^2}}}{e^{\frac{\sqrt{t}}{\lambda}}} \tag{A.16}$$

This may be rewritten as

$$T_{TC}(t) = T_\infty + c_1 \exp\left[\frac{\tau_0 \ln\left(\tau_0 + 2\lambda\sqrt{t}\right)}{2\lambda^2} - \frac{\sqrt{t}}{\lambda}\right] \tag{A.17}$$

Now, solving for c_1 at $t = 0$ yields

$$T_{TC}(t) = T_\infty + \frac{\left(T_{TC}(0) - T_\infty\right)}{\tau_0^{\frac{\tau_0}{2\lambda^2}}} \exp\left[\frac{\tau_0 \ln\left(\tau_0 + 2\lambda\sqrt{t}\right)}{2\lambda^2} - \frac{\sqrt{t}}{\lambda}\right] \tag{A.18}$$

Finally, after rearranging terms, the exact solution is obtained as

$$\theta_{TC}(t) = \frac{T_{TC}(t) - T_\infty}{T_{TC}(0) - T_\infty} = \exp\left\{\frac{1}{2\lambda^2}\left[\tau_0 \ln\left(\tau_0 + 2\lambda\sqrt{t}\right) - \tau_0 \ln\left(\tau_0\right) - 2\lambda\sqrt{t}\right]\right\}, \qquad t \geq 0, \tag{A.19}$$

A.2 EXPERIMENTAL SETUP PHOTOS

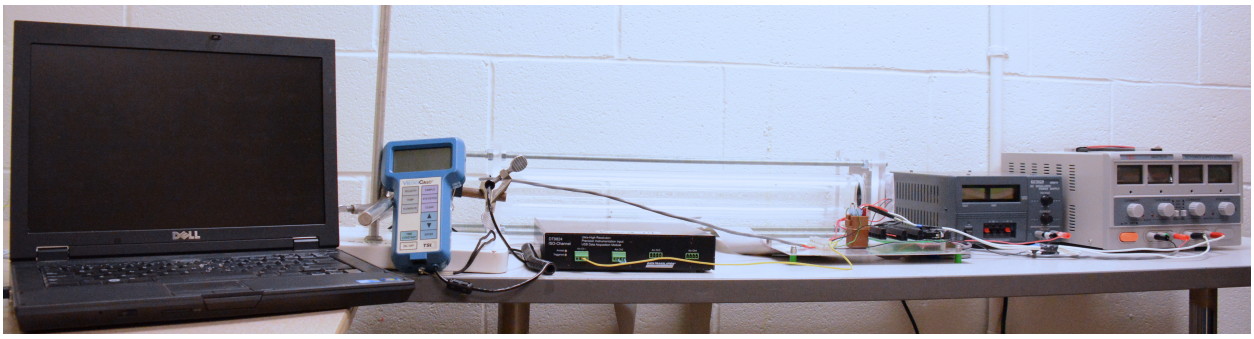

Figure A.2.1 Photo of the complete apparatus used to conduct LCSR tests on thermocouples in cross flow.

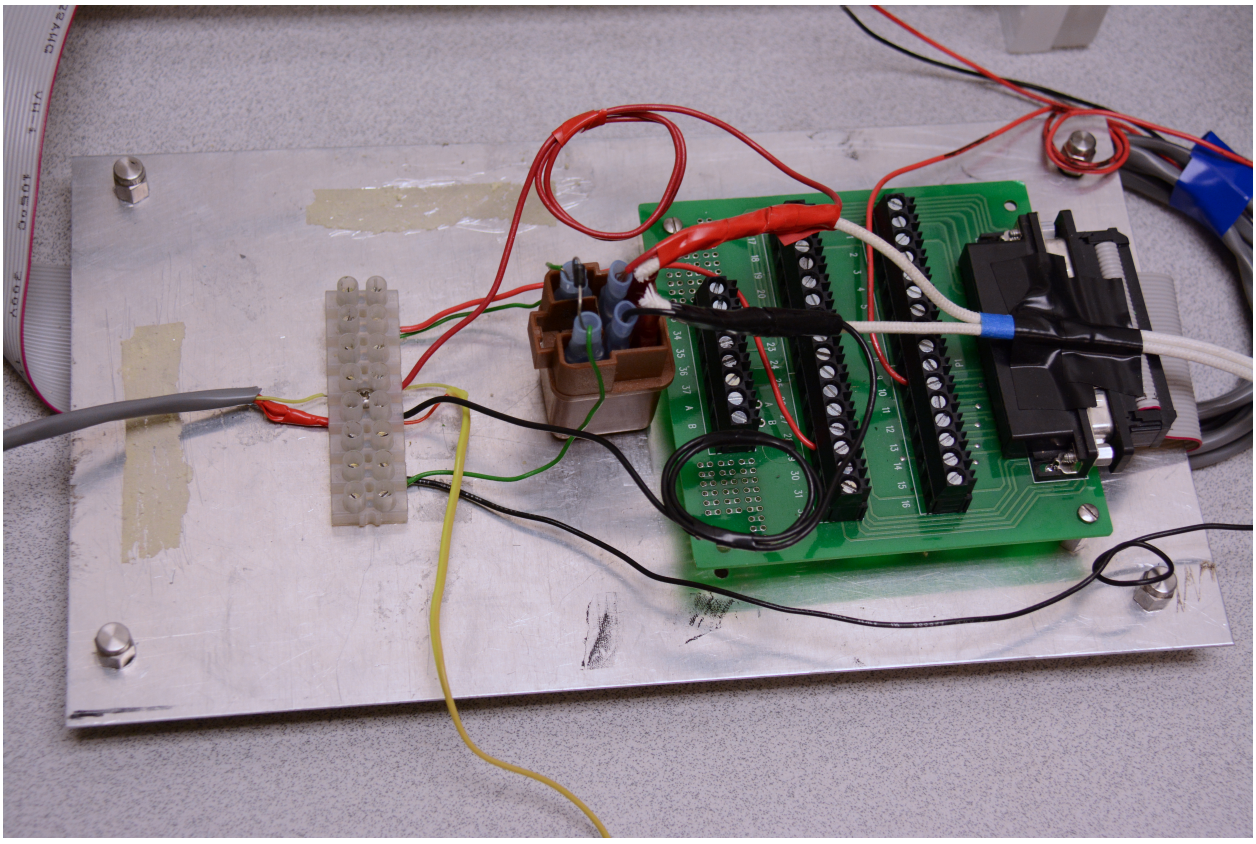

Figure A.2.2 Photo of the solid-state and mechanical relays used for LCSR testing.

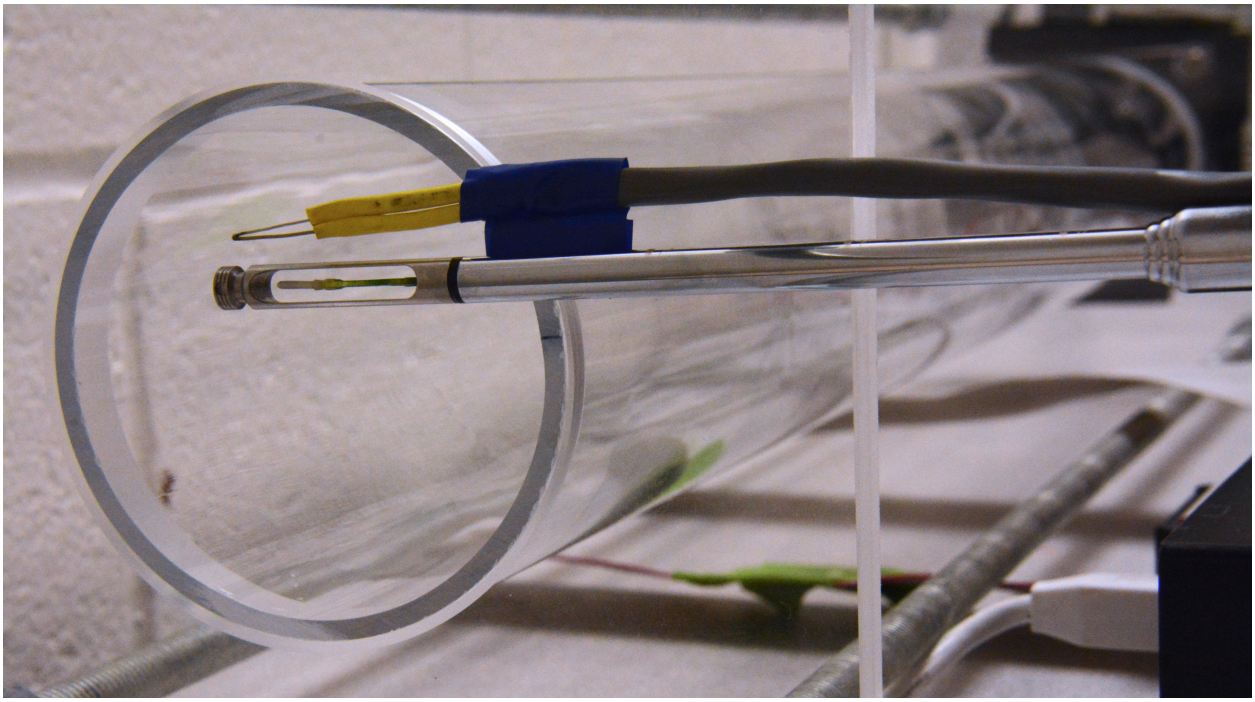

Figure A.2.3 Photo of a balanced-leads Type-K thermocouple and a hot-wire anemometer at the entrance of the flow channel.

A.3 LIST OF EXPERIMENTAL EQUIPMENT

-Dell Latitude E5400 Computer
-Data Translation DT9824 DAQ Board
-Data Translation DT9824 Solid-State Relay Module
-TSI VelociCalc 8345
-EXTECH 382213 DC Regulated Power Supply
-MASTECH HY3005D-2 DC Power Supply
-Nissan Mechanical Relay 25230 C9963 12V
-Delta Electronics, Inc. Model: AFB0812VHB DC Brushless Fan
-OMEGA Type-K Thermocouple Wire

VITA

Alexander Hashem Hashemian was born in Knoxville, Tennessee. He attended Webb School of Knoxville for ten years. Alexander graduated Magna Cum Laude with a Bachelors of Science degree in Mechanical Engineering from the University of Tennessee in December 2012. He has conducted heat transfer research for the Mechanical, Aerospace, and Biomedical Engineering Department of the University of Tennessee from January 2011 until May 2014. He is a member of the Tau Beta Pi Engineering Honor Society and the Pi Tau Sigma International Mechanical Engineering Honor Society. He intends to continue his education and ultimately pursue a career in the electrical power industry.